

REDUCED ORDER MODEL APPROACH TO INVERSE SCATTERING

LILIANA BORCEA*, VLADIMIR DRUSKIN†, ALEXANDER V. MAMONOV‡, MIKHAIL ZASLAVSKY§,
AND JÖRN ZIMMERLING¶

Abstract. We study an inverse scattering problem for a generic hyperbolic system of equations with an unknown coefficient called the reflectivity. The solution of the system models waves (sound, electromagnetic or elastic), and the reflectivity models unknown scatterers embedded in a smooth and known medium. The inverse problem is to determine the reflectivity from the time resolved scattering matrix (the data) measured by an array of sensors. We introduce a novel inversion method, based on a reduced order model (ROM) of an operator called wave propagator, because it maps the wave from one time instant to the next, at interval corresponding to the discrete time sampling of the data. The wave propagator is unknown in the inverse problem, but the ROM can be computed directly from the data. By construction, the ROM inherits key properties of the wave propagator, which facilitate the estimation of the reflectivity. The ROM was introduced previously and was used for two purposes: (1) to map the scattering matrix to that corresponding to the single scattering (Born) approximation and (2) to image i.e., obtain a qualitative estimate of the support of the reflectivity. Here we study further the ROM and show that it corresponds to a Galerkin projection of the wave propagator. The Galerkin framework is useful for proving properties of the ROM that are used in the new inversion method which seeks a quantitative estimate of the reflectivity.

Key words. Inverse scattering, model reduction, Galerkin approximation.

AMS subject classifications. 65M32, 41A20

1. Introduction. Consider an inverse scattering problem for a hyperbolic system of equations in symmetric form

$$\partial_t^2 \mathbf{u}(t, \mathbf{x}) + L(q)L(q)^T \mathbf{u}(t, \mathbf{x}) = 0, \quad \mathbf{x} \in \Omega, \quad t > 0, \quad (1.1)$$

$$\mathbf{u}(0, \mathbf{x}) = \mathbf{b}(\mathbf{x}), \quad \mathbf{x} \in \Omega, \quad (1.2)$$

$$\partial_t \mathbf{u}(0, \mathbf{x}) = \mathbf{0}, \quad (1.3)$$

satisfied by the wave $\mathbf{u}(t, \mathbf{x})$, where t denotes time and \mathbf{x} is the spatial variable in the domain $\Omega \subset \mathbb{R}^d$ in dimension $d \geq 1$, with piecewise smooth boundary $\partial\Omega$. The information about the medium is in the operator $L(q)$ and its adjoint $L(q)^T$, defined on spaces of functions satisfying some homogeneous boundary conditions. Both $L(q)$ and $L(q)^T$ are first order partial differential operators in the variable \mathbf{x} , with affine dependence on the unknown coefficient $q(\mathbf{x})$, called the reflectivity. The inverse problem is to determine $q(\mathbf{x})$ from data gathered by a collection (array) of sensors. This probes the medium with incident waves, determined by the initial condition $\mathbf{b}(\mathbf{x})$, and measures the backscattered waves.

Problem (1.1–1.3) arises in inverse scattering for sound, electromagnetic and elastic waves in isotropic media, as explained in [6, sections 3–5]. In acoustics, $\mathbf{u}(t, \mathbf{x})$ is related via some transformation to the scalar valued acoustic pressure, whereas in electromagnetics and elasticity, $\mathbf{u}(t, \mathbf{x})$ is related to the vector valued electric field and displacement velocity, respectively. The medium is modeled by variable coefficients in the wave equations: the wave speeds and wave impedances. Depending on the data acquisition setup, these coefficients affect in a different way the measurements at the array. Our definition of the reflectivity $q(\mathbf{x})$ takes this into account, as we now explain.

*Department of Mathematics, University of Michigan, Ann Arbor, MI 48109-1043 (borcea@umich.edu)

†Mathematical Sciences, Worcester Polytechnic Institute, Worcester, MA 01609-2280 (vdruskin@wpi.edu)

‡Department of Mathematics, University of Houston, Houston, TX 77004 (mamonov@math.uh.edu)

§Schlumberger-Doll Research Center, 1 Hampshire St., Cambridge, MA 02139-1578 (mzaslavsky@slb.com)

¶Department of Mathematics, University of Michigan, Ann Arbor, MI 48109-1043 (jzimmerl@umich.edu)

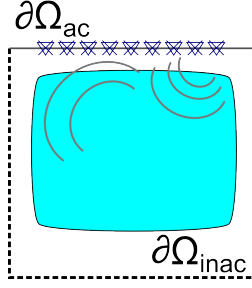


FIG. 1.1. *Illustration of the setup: An array of sensors (indicated with crosses) lying near the accessible boundary $\partial\Omega_{ac}$ probes an unknown medium with incident waves and measures the backscattered waves. The inaccessible boundary $\partial\Omega_{inac}$ is far enough from the sensors, so that it has no effect during the duration of the measurements.*

We consider the setup illustrated in Figure 1.1, where Ω is a cube in \mathbb{R}^d , obtained via truncation of a half space occupied by the unknown medium*. Assuming that the sensors record over the duration $t \in [0, T]$, and using that the wave speed is finite, we let the cube Ω have large enough side length, so that the measurements are not affected by the medium outside Ω . The boundary $\partial\Omega = \partial\Omega_{ac} \cup \partial\Omega_{inac}$ is the union of the accessible boundary $\partial\Omega_{ac}$, which is a subset of the boundary of the half space, and the inaccessible boundary $\partial\Omega_{inac}$. The name accessible means that the array of sensors can be placed in the immediate vicinity of $\partial\Omega_{ac}$. The inaccessible boundary is fictitious and has no effect on the measurements, so the backscattered wave is due entirely to reflectors contained in Ω . The initial condition in (1.2) is a vector valued function

$$\mathbf{b}(\mathbf{x}) = \left(b^{(1)}(\mathbf{x}), \dots, b^{(m)}(\mathbf{x}) \right), \quad (1.4)$$

where $b^{(s)}(\mathbf{x})$ is the wave emitted by one sensor[†]. It is a function supported in the vicinity of the sensor and the index $s = 1, \dots, m$ counts the sensors and the polarization of the wave.

The array measures the scattering matrix (the data), modeled by [6, sections 3-5]

$$\mathbf{D}_j = \langle \mathbf{b}, \mathbf{u}(j\tau, \cdot) \rangle = \int_{\Omega} d\mathbf{x} \mathbf{b}(\mathbf{x})^T \mathbf{u}(j\tau, \mathbf{x}), \quad j = 0, \dots, 2n - 1. \quad (1.5)$$

The s^{th} column of this symmetric $m \times m$ matrix corresponds to the wave generated by $b^{(s)}(\mathbf{x})$ and evaluated at all the sensors in the array, at time instant $j\tau$, where $\tau > 0$ is chosen consistent with the Nyquist sampling rate of the wave.

The wave $\mathbf{u}(t, \mathbf{x})$ and therefore the data (1.5) depend in a complicated, nonlinear way on the coefficients (wave speed and impedance) of the wave equation. The low spatial frequency component of the wave speed determines the kinematics of the wave [23, 4], since time of travel is a path integral of the slowness (the reciprocal of the velocity). The estimation of this smooth part (aka the kinematic model) is of great interest in geophysical exploration [23]. It is a difficult problem in the backscattering setup considered here and at high frequencies used in applications, because nearby models can give travel time discrepancies that exceed

*One can also consider truncation of the whole space, as long as the medium is known and non-scattering on one side of the array of sensors.

[†]Note that typically, the source excitation is expressed as a time dependent force in the right hand-side of the wave equation, with homogeneous initial conditions. We refer to appendix A for the derivation of the initial value problem (1.1)–(1.3) from such a formulation. We also give there the expression of $\mathbf{b}(\mathbf{x})$ which depends on the waveform emitted by the source.

the short period of oscillation of the wave. Thus, unless data have low temporal frequencies, typical least squares data fit optimization formulations [25] are not amenable to solutions by Newton-type methods [26]. Other approaches have emerged [22], and they use redundant data sets to separate the estimation of the kinematic model and the rough, backscattering part of the medium, called the reflectivity. We assume that the kinematic model is known[‡] and is such that the wave front advances forward (there are no lensing effects). Then, the study in [2] shows that if the depth of the reflectors is larger than the diameter of the array, backscattering is mostly due to relative variations of the wave impedance. This motivates our definition of $q(\mathbf{x})$ as the logarithm of the impedance [6, sections 3-5].

The estimation of the reflectivity from backscattering data i.e., inverting the mapping

$$q \mapsto \{\mathbf{D}_j, j = 0, \dots, 2n - 1\}, \quad (1.6)$$

has applications in nondestructive testing [20], ultrasound for medical diagnostics [24], radar [8], geophysical exploration [23], underwater sonar [10], and so on. It is a nonlinear inverse problem, even though $L(q)$ is affine in $q(\mathbf{x})$, as can be seen by solving (1.1–1.3)

$$\mathbf{u}(t, \mathbf{x}) = \cos\left(t\sqrt{L(q)L(q)^T}\right)\mathbf{b}(\mathbf{x}), \quad t > 0, \quad (1.7)$$

and substituting the solution in the data model (1.5)

$$\mathbf{D}_j = \left\langle \mathbf{b}, \cos\left(j\tau\sqrt{L(q)L(q)^T}\right)\mathbf{b} \right\rangle, \quad j = 0, \dots, 2n - 1, \quad (1.8)$$

where the square root and cosine are defined as usual, using the spectral decomposition of the self-adjoint, nonnegative-definite operator $L(q)L(q)^T$. Basically all existing algorithms search for the reflectivity with a least squares data fit optimization formulation, and in many applications the mapping (1.6) is linearized i.e., $q(\mathbf{x})$ is estimated by the solution of the normal equation. The normal operator is not invertible in general, but in many setups it has the property that it preserves approximately the location of non-smooth features of $q(\mathbf{x})$, like jumps [23]. Therefore, popular methods like reverse time migration [9, 3, 4] and the related backprojection [1, 8] use the right hand side of the normal equation as an image, i.e., an estimate of the support of $q(\mathbf{x})$. These imaging methods work well if the reflectivity $q(\mathbf{x})$ is weak, but they are qualitative. A quantitative estimate of a general reflectivity requires inverting, in an appropriate sense, the nonlinear map (1.6).

We propose a method for estimating $q(\mathbf{x})$ based on a reduced order model (ROM) of the self-adjoint wave propagator operator

$$\mathcal{P}(q) = \cos\left(\tau\sqrt{L(q)L(q)^T}\right). \quad (1.9)$$

This operator is useful because it allows us to view the wave $\mathbf{u}(j\tau, \mathbf{x})$ as the state of a discrete dynamical system, starting from $\mathbf{b}(\mathbf{x})$ and evolving with the time index $j \geq 0$. We can write explicitly the state $\mathbf{u}(j\tau, \mathbf{x}) = \mathcal{T}_j(\mathcal{P}(q))\mathbf{b}(\mathbf{x})$ using equations (1.7) and (1.9), and substituting in the expression (1.8) of the data we obtain

$$\mathbf{D}_j = \langle \mathbf{b}, \cos(j \arccos \mathcal{P}(q))\mathbf{b} \rangle = \langle \mathbf{b}, \mathcal{T}_j(\mathcal{P}(q))\mathbf{b} \rangle, \quad j = 0, \dots, 2n - 1, \quad (1.10)$$

where \mathcal{T}_j are Chebyshev polynomials of the first kind [19]. The ROM is defined by a pair of matrices $\mathcal{P}^{\text{ROM}}(q) \in \mathbb{R}^{nm \times nm}$ and $\mathbf{b}^{\text{ROM}} \in \mathbb{R}^{nm \times m}$, which are proxies of $\mathcal{P}(q)$ and $\mathbf{b}(\mathbf{x})$,

[‡]The kinematic model (smooth wave speed) appears in the coefficients of the operators $L(q)$ and $L(q)^T$ (see [6] and sections 3–4). We suppress the dependence on the known kinematic model in our notation.

in the sense that they define a dynamical system for the discrete state $\mathcal{T}_j(\mathcal{P}^{\text{ROM}}(q))\mathbf{b}^{\text{ROM}}$, that encodes essential features of $\mathbf{u}(j\tau, \mathbf{x})$ and satisfies

$$\mathbf{D}_j = \langle \mathbf{b}, \mathcal{T}_j(\mathcal{P}(q))\mathbf{b} \rangle = \mathbf{b}^{\text{ROM}T} \mathcal{T}_j(\mathcal{P}^{\text{ROM}}(q))\mathbf{b}^{\text{ROM}}, \quad j = 0, \dots, 2n - 1. \quad (1.11)$$

The matrices $\mathcal{P}^{\text{ROM}}(q)$ and \mathbf{b}^{ROM} satisfying (1.11) are calculated from the data (1.8) (i.e., the ROM is data-driven) and they capture physical aspects of the wave propagation that are needed for inversion. The ROM was introduced in [13, 6] and was used in [14] for imaging, and in [5] for transforming the data (1.8) to that corresponding to the single scattering (Born) approximation. The new results in this paper are:

1. We show that the ROM propagator $\mathcal{P}^{\text{ROM}}(q)$ is a Galerkin projection of the operator (1.9), and use the Galerkin framework to prove properties of the ROM that facilitate the solution of the inverse scattering problem.
2. We use the ROM to develop a novel, quantitative inversion method for estimating $q(\mathbf{x})$. The data are fit implicitly in our method, and the inversion is formulated as a minimization of the discrepancy between the data-driven ROM and the ROM calculated for the search reflectivity. This optimization problem turns out to be almost linear i.e., it can be solved in very few iterations, and it is better conditioned than the classic least squares data fit approach.

The paper is organized as follows: In section 2 we describe the ROM in the Galerkin framework and analyze its properties, which are then used in section 3 to introduce the new inversion method. We assess the performance of the method with numerical simulations in section 4. The presentation in section 2 does not depend on the expression of the operator $L(q)$ and its adjoint, so we work with the generic hyperbolic system (1.1–1.3). However, the inversion algorithm requires specifying $L(q)$, so in sections 3–4 we use the operator derived from the acoustic wave equation. We end with a summary in section 5.

2. The Galerkin framework. To introduce the Galerkin framework, consider the approximation space

$$\mathfrak{X} = \text{colspan}\{\mathbf{u}(j\tau, \mathbf{x}), j = 0, \dots, n - 1\}, \quad (2.1)$$

where

$$\mathbf{u}(j\tau, \mathbf{x}) = \left(u^{(1)}(j\tau, \mathbf{x}), \dots, u^{(m)}(j\tau, \mathbf{x}) \right), \quad j \geq 0, \quad (2.2)$$

are the solution snapshots, with components

$$u^{(s)}(j\tau, \mathbf{x}) = \cos\left(j\tau\sqrt{L(q)L(q)^T}\right)b^{(s)}(\mathbf{x}), \quad s = 1, \dots, m. \quad (2.3)$$

We begin in section 2.1 with an exact time stepping scheme satisfied by these snapshots, which shows the role of the propagator operator (1.9). The ROM is defined from the Galerkin approximation of this time stepping scheme, as explained in section 2.2. Note that the approximation space \mathfrak{X} is not known in inversion, because the data (1.5) correspond to the snapshots evaluated at the locations of the sensors, and not inside the medium. Nevertheless, it is possible to compute the ROM, as explained in section 2.3. The properties of the ROM are stated in section 2.4 and are proved in appendices B–E. In section 2.5 we explain that there is a family of ROMs that share these properties, and that they are connected by special orthogonal transformations. We also give in section 2.6 an intuitive, finite differences interpretation of the ROM, which is then used in section 3 to motivate the inversion algorithm.

2.1. The propagator and time stepping. Let us introduce the notation

$$\mathbf{u}_j(\mathbf{x}) = \mathbf{u}(j\tau, \mathbf{x}), \quad j \geq 0, \quad (2.4)$$

and obtain from the definition (2.2-2.3) and the trigonometric identity satisfied by the cosine, that the snapshots satisfy the time stepping scheme

$$\mathbf{u}_{j+1}(\mathbf{x}) = 2\mathcal{P}(q)\mathbf{u}_j(\mathbf{x}) - \mathbf{u}_{j-1}(\mathbf{x}), \quad j \geq 0, \quad (2.5)$$

$$\mathbf{u}_0(\mathbf{x}) = \mathbf{b}(\mathbf{x}), \quad (2.6)$$

$$\mathbf{u}_1(\mathbf{x}) = \mathbf{u}_{-1}(\mathbf{x}). \quad (2.7)$$

This justifies calling $\mathcal{P}(q)$ the wave propagator operator, because it is used to map the wave at consecutive time instants $(j-1)\tau$ and $j\tau$, to the wave at future time $(j+1)\tau$.

Note that (2.5) is the three term recursion relation satisfied by the orthogonal Chebyshev polynomials \mathcal{T}_j and indeed, definitions (1.9) and (2.2-2.3) give

$$\mathbf{u}_j(\mathbf{x}) = \cos(j \arccos \mathcal{P}(q))\mathbf{b}(\mathbf{x}) = \mathcal{T}_j(\mathcal{P}(q))\mathbf{b}(\mathbf{x}), \quad j \geq 0. \quad (2.8)$$

Note also that if we subtract $2\mathbf{u}_j(\mathbf{x})$ from equation (2.5) and divide the result by τ^2 we obtain the second order time stepping scheme

$$\frac{\mathbf{u}_{j+1}(\mathbf{x}) - 2\mathbf{u}_j(\mathbf{x}) + \mathbf{u}_{j-1}(\mathbf{x})}{\tau^2} + \mathcal{L}(q)\mathcal{L}(q)^T\mathbf{u}_j(\mathbf{x}) = 0, \quad j \geq 0, \mathbf{x} \in \Omega, \quad (2.9)$$

$$\mathbf{u}_0(\mathbf{x}) = \mathbf{b}(\mathbf{x}), \quad (2.10)$$

$$\mathbf{u}_1(\mathbf{x}) = \mathbf{u}_{-1}(\mathbf{x}), \quad (2.11)$$

where $\mathcal{L}(q)$ is the square root of the self-adjoint, non-negative definite operator

$$\frac{2}{\tau^2}(I - \mathcal{P}(q)) = \mathcal{L}(q)\mathcal{L}(q)^T, \quad (2.12)$$

and I denotes the identity. Equations (2.9–2.11) are an exact time stepping scheme for the hyperbolic problem (1.1–1.3), with boundary conditions taken into account in the definition of $L(q)$ and $L(q)^T$. The derivative $\partial_t^2 \mathbf{u}(j\tau, \mathbf{x})$ is replaced in (2.9) by second order centered differences, and the $O(\tau^2)$ error is absorbed in the operator $\mathcal{L}(q)$ which approximates $L(q)$. That is to say, $\mathcal{L}(q)\mathcal{L}(q)^T$ has the same eigenfunctions as $L(q)L(q)^T$, and the eigenvalues

$$\frac{2}{\tau^2}[1 - \cos(\tau\sqrt{\theta})] = \theta[1 + O(\tau^2\theta)],$$

where $\theta > 0$ denotes an eigenvalue of $L(q)L(q)^T$. The larger part of the spectrum corresponds to more oscillatory eigenfunctions[§], so the restrictions of $\mathcal{L}(q)\mathcal{L}(q)^T$ and $L(q)L(q)^T$ on the space of functions that oscillate at smaller spatial frequency $\lesssim 1/(c_o\tau)$, where c_o is a reference wave speed, are approximately the same.

2.2. Galerkin approximation. We define the ROM using the Galerkin approximation of (2.5–2.7), under the following assumption:

ASSUMPTION 2.1. *The solution snapshots (2.2-2.3) are linearly independent up to time $n\tau$. This implies that the approximation space (2.1) has dimension nm .*

The linear independence of the snapshots can be ensured initially by having sufficiently well separated sensors in the array (recall that the components of (1.4) are approximations of

[§]For the purpose of the explanation, we may think of $L(q)L(q)^T$ as the negative Laplacian multiplied by c_o^2 .

the delta function at the sensor locations). However, depending on the kinematic model, the waves may focus at later time in some region of the domain, or they may turn around, and the snapshots can become linearly dependent. We assume in the analysis that the medium is nice enough such that Assumption 2.1 holds, but in the ROM construction and inversion we can deal with a lower dimensional approximation space using an SVD truncation.

Let us gather the first n snapshots in the quasimatrix

$$\mathbf{U}(\mathbf{x}) = (\mathbf{u}_0(\mathbf{x}), \dots, \mathbf{u}_{n-1}(\mathbf{x})), \quad (2.13)$$

with nm linearly independent columns that span the approximation space (2.1). Following [21], by quasimatrix we mean a row vector valued function defined on Ω , with the entry index viewed as a column index and $\mathbf{x} \in \Omega$ playing the role of a row index. The quasimatrix $\mathbf{U}(\mathbf{x})$ is organized in (2.13) in n blocks, each with m entries.

Using linear algebra terminology, we write

$$\mathfrak{X} = \text{range}(\mathbf{U}(\mathbf{x})), \quad (2.14)$$

and we call henceforth the components of quasimatrices like (2.13) block columns. The Galerkin approximation of the snapshots is

$$\mathbf{u}_j(\mathbf{x}) \approx \mathbf{U}(\mathbf{x})\mathbf{g}_j, \quad j \geq 0, \quad (2.15)$$

where $\mathbf{g}_j \in \mathbb{R}^{nm \times m}$ is the matrix of Galerkin coefficients. These are calculated so that when substituting (2.15) in (2.5), the residual is orthogonal to the space (2.14)

$$\langle \mathbf{u}_l, \mathbf{U}\mathbf{g}_{j+1} - 2\mathcal{P}(q)\mathbf{U}\mathbf{g}_j + \mathbf{U}\mathbf{g}_{j-1} \rangle = \mathbf{0}, \quad \forall l = 0, \dots, n-1, \quad (2.16)$$

where we recall the definition of $\langle \cdot, \cdot \rangle$ from (1.5).

By construction, the approximation (2.15) is exact for $j = 0, \dots, n-1$, so

$$\mathbf{g}_j = \mathbf{e}_j = (\mathbf{0}_m, \dots, \mathbf{0}_m, \mathbf{I}_m, \mathbf{0}_m, \dots, \mathbf{0}_m)^T, \quad j = 0, \dots, n-1, \quad (2.17)$$

are the matrices of size $nm \times m$ with an $m \times m$ identity \mathbf{I}_m at block position j , and all other blocks being $m \times m$ zero matrices $\mathbf{0}_m$.[¶] Using this observation and rewriting (2.16) in matrix form, we obtain the Galerkin time stepping scheme

$$\mathbf{M}\mathbf{g}_{j+1} = 2\mathbf{S}\mathbf{g}_j - \mathbf{M}\mathbf{g}_{j-1}, \quad j \geq 0, \quad (2.18)$$

$$\mathbf{g}_0 = \mathbf{e}_0, \quad (2.19)$$

$$\mathbf{g}_1 = \mathbf{g}_{-1} = \mathbf{e}_1, \quad (2.20)$$

with mass matrix

$$\mathbf{M} = \mathbf{U}^T \mathbf{U} \in \mathbb{R}^{nm \times nm}, \quad (2.21)$$

and stiffness matrix

$$\mathbf{S} = \mathbf{U}^T \mathcal{P}(q)\mathbf{U} \in \mathbb{R}^{nm \times nm}. \quad (2.22)$$

Again, we use linear algebra notation, where for all $\mathbf{W}(\mathbf{x}) = (\mathbf{w}_0(\mathbf{x}), \dots, \mathbf{w}_{n-1}(\mathbf{x}))$ lying in the same space as $\mathbf{U}(\mathbf{x})$, we denote by $\mathbf{U}^T \mathbf{W}$ the $nm \times nm$ matrix with $m \times m$ blocks

$$(\mathbf{U}^T \mathbf{W})_{i,j} = \langle \mathbf{u}_i, \mathbf{w}_j \rangle, \quad i, j = 0, \dots, n-1. \quad (2.23)$$

[¶]Note that for convenience we count the block entries starting from 0.

2.2.1. Definition of the ROM. We conclude from Assumption 2.1 and definition (2.21) that the mass matrix is symmetric and positive definite, so we can take its square root using the block Cholesky factorization [15, Chapter 4],

$$M = \mathbf{R}^T \mathbf{R}, \quad (2.24)$$

where $\mathbf{R} \in \mathbb{R}^{nm \times nm}$ is block upper triangular, with $m \times m$ blocks. This matrix is invertible, and multiplying (2.18) on the left by \mathbf{R}^{-T} (the transpose of the inverse of \mathbf{R}), we obtain the ROM version of the time stepping scheme (2.5–2.7),

$$\mathbf{u}_{j+1}^{\text{ROM}} = 2\mathcal{P}^{\text{ROM}}(q)\mathbf{u}_j^{\text{ROM}} - \mathbf{u}_{j-1}^{\text{ROM}}, \quad j \geq 0, \quad (2.25)$$

$$\mathbf{u}_0^{\text{ROM}} = \mathbf{b}^{\text{ROM}}, \quad (2.26)$$

$$\mathbf{u}_1^{\text{ROM}} = \mathbf{u}_{-1}^{\text{ROM}} = \mathbf{R}\mathbf{e}_1, \quad (2.27)$$

satisfied by the ROM snapshots

$$\mathbf{u}_j^{\text{ROM}} = \mathbf{R}\mathbf{g}_j, \quad j \geq 0. \quad (2.28)$$

The ROM propagator is the $nm \times nm$ symmetric matrix

$$\mathcal{P}^{\text{ROM}}(q) = \mathbf{R}^{-T} \mathbf{S} \mathbf{R}^{-1}, \quad (2.29)$$

and the initial snapshot is the $nm \times m$ matrix

$$\mathbf{b}^{\text{ROM}} = \mathbf{R}\mathbf{g}_0 = \mathbf{R}\mathbf{e}_0. \quad (2.30)$$

2.2.2. Galerkin projection. Let us use the quasimatrix of snapshots (2.13) and the inverse of the Cholesky factor \mathbf{R} of the mass matrix to define the new quasimatrix

$$\mathbf{V}(\mathbf{x}) = \mathbf{U}(\mathbf{x})\mathbf{R}^{-1} = (\mathbf{v}_0(\mathbf{x}), \dots, \mathbf{v}_{n-1}(\mathbf{x})). \quad (2.31)$$

The nm columns of this quasimatrix are organized in the blocks

$$\mathbf{v}_j(\mathbf{x}) = \mathbf{U}(\mathbf{x})\mathbf{R}^{-1}\mathbf{e}_j, \quad j = 0, \dots, n-1, \quad (2.32)$$

and they form an orthonormal basis of the approximation space (2.14). This follows from definitions (2.21), (2.32) and the Cholesky factorization (2.24),

$$\mathbf{V}^T \mathbf{V} = \mathbf{R}^{-T} \mathbf{U}^T \mathbf{U} \mathbf{R}^{-1} = \mathbf{I}_{nm}, \quad (2.33)$$

where \mathbf{I}_{nm} is the $nm \times nm$ identity matrix and we used the linear algebra notation (2.23). Therefore, the block columns (2.32) of $\mathbf{V}(\mathbf{x})$ are called the orthonormal snapshots.

We now see that the ROM propagator is the projection of $\mathcal{P}(q)$ on the approximation space (2.1), written in the basis of the orthonormal snapshots,

$$\mathcal{P}^{\text{ROM}}(q) \stackrel{(2.29)}{=} \mathbf{R}^{-T} \mathbf{S} \mathbf{R}^{-1} \stackrel{(2.22)}{=} \mathbf{R}^{-T} \mathbf{U}^T \mathcal{P}(q) \mathbf{U} \mathbf{R}^{-1} \stackrel{(2.31)}{=} \mathbf{V}^T \mathcal{P}(q) \mathbf{V}. \quad (2.34)$$

Moreover, the initial ROM snapshot (2.30) is the projection of the initial wave,

$$\mathbf{b}^{\text{ROM}} \stackrel{(2.30)}{=} \mathbf{R}\mathbf{e}_0 = \mathbf{V}^T \mathbf{U} \mathbf{e}_0 = \mathbf{V}^T \mathbf{b}, \quad (2.35)$$

because $\mathbf{U}(\mathbf{x})\mathbf{e}_0 = \mathbf{b}(\mathbf{x})$ and equations (2.31) and (2.33) give $\mathbf{R} = \mathbf{V}^T \mathbf{U}$.

REMARK 2.2. Definition (2.31) of $\mathbf{V}(\mathbf{x})$ is the Gram-Schmidt orthogonalization of the snapshots. It is a causal construction of the orthonormal basis

$$\mathbf{v}_j(\mathbf{x}) \in \text{span}\{\mathbf{u}_0(\mathbf{x}), \dots, \mathbf{u}_j(\mathbf{x})\}, \quad \forall j = 0, \dots, n-1, \quad (2.36)$$

that respects the physics of the wave propagation, captured by the ROM time stepping scheme (2.25–2.27). Indeed, (2.35) and the block upper triangular structure of \mathbf{R} give that only the first block of \mathbf{b}^{ROM} is non-zero. This corresponds to the initial wave $\mathbf{b}(\mathbf{x})$ being supported near the array. The wavefront of $\mathbf{u}(t, \mathbf{x})$ penetrates deeper inside the medium for later time, and this is reflected in the algebraic structure of the ROM snapshots (2.28), where the rows of blocks are filled in sequentially, for each time step. In particular, we obtain from (2.17), (2.28) and (2.31) that

$$(\mathbf{u}_0^{\text{ROM}}, \dots, \mathbf{u}_{n-1}^{\text{ROM}}) = \mathbf{R} = \mathbf{V}^T \mathbf{U} = \mathbf{V}^T (\mathbf{u}_0, \dots, \mathbf{u}_{n-1}). \quad (2.37)$$

The importance of this remark will become clear in sections 2.4 and 2.6, where we show how the causality preserving definition of the ROM induces properties of $\mathcal{P}^{\text{ROM}}(q)$ that are useful for solving the inverse scattering problem.

2.3. Data-driven ROM. In inverse scattering we do not know the snapshots, so how can we use the definition (2.29–2.30) of the ROM? We now explain that, in fact, the mass and stiffness matrices can be calculated from the data (1.8). Consequently, we can compute the ROM from (2.29–2.30) and we can also get the ROM snapshots via the time stepping scheme (2.25–2.27). Furthermore, we can use equation (2.28) to calculate the Galerkin coefficients in the approximation (2.15), without knowing the approximation space (2.1).

Here we recall the calculation of mass and stiffness matrices from the data introduced in [5, 13] that we repeat for the convenience of the reader. The blocks of the mass matrix are, by definition (2.21) and equation (2.8),

$$\mathbf{M}_{i,j} = \langle \mathcal{T}_i(\mathcal{P}(q))\mathbf{b}, \mathcal{T}_j(\mathcal{P}(q))\mathbf{b} \rangle = \langle \mathbf{b}, \mathcal{T}_i(\mathcal{P}(q))\mathcal{T}_j(\mathcal{P}(q))\mathbf{b} \rangle, \quad (2.38)$$

where the last equality is because $\mathcal{P}(q)$ is self-adjoint. The Chebyshev polynomials of an arbitrary argument z have the multiplicative property

$$\mathcal{T}_i(z)\mathcal{T}_j(z) = \frac{1}{2} [\mathcal{T}_{i+j}(z) + \mathcal{T}_{|i-j|}(z)], \quad (2.39)$$

so using this property in (2.38) and recalling (1.10) we obtain

$$\mathbf{M}_{i,j} = \frac{1}{2} \left[\langle \mathbf{b}, \mathcal{T}_{i+j}(\mathcal{P}(q))\mathbf{b} \rangle + \langle \mathbf{b}, \mathcal{T}_{|i-j|}(\mathcal{P}(q))\mathbf{b} \rangle \right] \quad (2.40)$$

$$= \frac{1}{2} (\mathbf{D}_{i+j} + \mathbf{D}_{|i-j|}), \quad i, j = 0, \dots, n-1. \quad (2.41)$$

The calculation of \mathbf{S} is similar. Starting with its definition (2.22) and using equation (2.8), we have

$$\mathbf{S}_{i,j} = \langle \mathcal{T}_i(\mathcal{P}(q))\mathbf{b}, \mathcal{P}(q)\mathcal{T}_j(\mathcal{P}(q))\mathbf{b} \rangle = \langle \mathbf{b}, \mathcal{T}_i(\mathcal{P}(q))\mathcal{P}(q)\mathcal{T}_j(\mathcal{P}(q))\mathbf{b} \rangle, \quad (2.42)$$

where by the multiplicative property (2.39),

$$z\mathcal{T}_j(z) = \mathcal{T}_1(z)\mathcal{T}_j(z) = \frac{1}{2} [\mathcal{T}_{j+1}(z) + \mathcal{T}_{|j-1|}(z)].$$

Substituting in (2.42), using (2.39) one more time, and recalling (1.10), we get

$$\mathbf{S}_{i,j} = \frac{1}{4} (\mathbf{D}_{i+j+1} + \mathbf{D}_{|i-j+1|} + \mathbf{D}_{|i+j-1|} + \mathbf{D}_{|i-j-1|}), \quad i, j = 0, \dots, n-1. \quad (2.43)$$

2.4. Properties of the ROM. We state here the theorems that describe the properties of the ROM. To lighten the presentation, we write the proofs in the appendixes.

2.4.1. Data fit. We saw in the previous section how the ROM is calculated from the data. The next theorem, proved in appendix B, states that the ROM fits exactly these data.

THEOREM 2.3. *The ROM snapshots (2.28) can be written as Chebyshev polynomials of the ROM propagator, similar to (2.8),*

$$\mathbf{u}_j^{\text{ROM}} = \mathcal{T}_j(\mathcal{P}^{\text{ROM}}(q))\mathbf{b}^{\text{ROM}}, \quad j \geq 0, \quad (2.44)$$

and the ROM defined by (2.29–2.30) satisfies the data fit relations (1.11).

Recall from section 2.2 that the first n snapshots are represented exactly in our Galerkin scheme. Therefore, it is not surprising that the ROM fits the data for the first n time instants. The interesting point of the theorem is that the data are fit for the remaining n time instants. Physically, this is because the measurements at the array of duration $(2n - 1)\tau$ can only sense the medium up to the depth traveled by waves in half the time, and all this information is contained in our approximation space (2.14). This can be seen from the following equation

$$\begin{aligned} D_{n-1+j} &= \langle \mathbf{b}, \mathcal{T}_{n-1+j}(\mathcal{P}(q))\mathbf{b} \rangle \\ &= 2 \langle \mathbf{b}, \mathcal{T}_{n-1}(\mathcal{P}(q))\mathcal{T}_j(\mathcal{P}(q))\mathbf{b} \rangle - \langle \mathbf{b}, \mathcal{T}_{|n-1-j|}(\mathcal{P}(q))\mathbf{b} \rangle \\ &= 2 \langle \mathbf{u}_{n-1}, \mathbf{u}_j \rangle - \langle \mathbf{b}, \mathbf{u}_{|n-1-j|} \rangle, \end{aligned}$$

obtained using the recursion relation of Chebyshev polynomials, equation (2.8) and the self-adjointness of $\mathcal{P}(q)$. Indeed, if $j = 1, \dots, n - 1$, the right hand side can be calculated in terms of the waves $\{\mathbf{u}_l(\mathbf{x})\}_{0 \leq l \leq n-1}$. In fact, this is the case even for $j = n$, as shown by a more involved calculation given in appendix B.

2.4.2. ROM factorization. Just as we did in section (2.1), we can subtract $2\mathbf{u}_j^{\text{ROM}}$ from equation (2.25) and divide the result by τ^2 to obtain the ROM equivalent of the second order time stepping scheme (2.9–2.11),

$$\frac{\mathbf{u}_{j+1}^{\text{ROM}} - 2\mathbf{u}_j^{\text{ROM}} + \mathbf{u}_{j-1}^{\text{ROM}}}{\tau^2} + \mathcal{L}^{\text{ROM}}(q)\mathcal{L}^{\text{ROM}}(q)^T \mathbf{u}_j^{\text{ROM}} = 0, \quad j \geq 0, \quad (2.45)$$

$$\mathbf{u}_0^{\text{ROM}} = \mathbf{b}^{\text{ROM}}, \quad (2.46)$$

$$\mathbf{u}_1^{\text{ROM}} = \mathbf{u}_{-1}^{\text{ROM}}, \quad (2.47)$$

with matrix $\mathcal{L}^{\text{ROM}}(q)$ defined by the block Cholesky factorization

$$\frac{2}{\tau^2}(\mathbf{I}_{nm} - \mathcal{P}^{\text{ROM}}(q)) = \mathcal{L}^{\text{ROM}}(q)\mathcal{L}^{\text{ROM}}(q)^T. \quad (2.48)$$

This is the ROM analogue of the factorization

$$\frac{2}{\tau^2}(I - \mathcal{P}(q)) = \mathcal{L}(q)\mathcal{L}(q)^T \approx L(q)L(q)^T, \quad (2.49)$$

where the approximation is as discussed in section (2.1).

The next theorem, proved in appendix C, gives that the ROM propagator is a block tridiagonal invertible matrix. We return to this point in section 2.6, where we explain that the block tridiagonal $\mathcal{L}^{\text{ROM}}(q)\mathcal{L}^{\text{ROM}}(q)^T$ can be viewed as a finite difference approximation of the second order partial differential operator $L(q)L(q)^T$.

THEOREM 2.4. *The ROM propagator $\mathcal{P}^{\text{ROM}}(q)$ is symmetric, block tridiagonal and the matrix $\mathbf{I}_{nm} - \mathcal{P}^{\text{ROM}}(q)$ is invertible. Therefore, the Cholesky factor $\mathcal{L}^{\text{ROM}}(q)$ is an invertible matrix with lower block bidiagonal structure.*

2.4.3. Galerkin-Petrov projection. We now show that $\mathcal{L}^{\text{ROM}}(q)$ is a Galerkin-Petrov projection of the operator $\mathcal{L}(q)$ on the subspace \mathfrak{X} defined in (2.1) and the subspace

$$\widehat{\mathfrak{X}} = \text{span}\{\widehat{\mathbf{u}}_0(\mathbf{x}), \dots, \widehat{\mathbf{u}}_{n-1}(\mathbf{x})\}, \quad (2.50)$$

of the first n dual snapshots denoted by the hat.

The dual snapshots are defined using the first order system formulation of the time stepping scheme (2.9–2.11),

$$\frac{\mathbf{u}_{j+1}(\mathbf{x}) - \mathbf{u}_j(\mathbf{x})}{\tau} = -\mathcal{L}(q)\widehat{\mathbf{u}}_j(\mathbf{x}), \quad (2.51)$$

$$\frac{\widehat{\mathbf{u}}_j(\mathbf{x}) - \widehat{\mathbf{u}}_{j-1}(\mathbf{x})}{\tau} = \mathcal{L}(q)^T \mathbf{u}_j(\mathbf{x}), \quad j \geq 0, \quad (2.52)$$

$$\mathbf{u}_0(\mathbf{x}) = \mathbf{b}(\mathbf{x}) \quad (2.53)$$

$$\widehat{\mathbf{u}}_0(\mathbf{x}) + \widehat{\mathbf{u}}_{-1}(\mathbf{x}) = 0. \quad (2.54)$$

Indeed, it is easy to check that (2.51–2.54) implies (2.9–2.10) and the initial condition (2.11) follows from

$$\begin{aligned} \frac{\mathbf{u}_{-1}(\mathbf{x}) - \mathbf{u}_1(\mathbf{x})}{\tau} &= -\frac{\mathbf{u}_1(\mathbf{x}) - \mathbf{u}_0(\mathbf{x})}{\tau} - \frac{\mathbf{u}_0(\mathbf{x}) - \mathbf{u}_{-1}(\mathbf{x})}{\tau} \\ &\stackrel{(2.51)}{=} \mathcal{L}(q)(\widehat{\mathbf{u}}_0(\mathbf{x}) + \widehat{\mathbf{u}}_{-1}(\mathbf{x})) \stackrel{(2.54)}{=} 0. \end{aligned}$$

The first dual snapshot is obtained from (2.52) evaluated at $j = 0$ and (2.54),

$$\widehat{\mathbf{u}}_0(\mathbf{x}) = \widehat{\mathbf{b}}(\mathbf{x}) = \frac{\tau}{2} \mathcal{L}(q)^T \mathbf{b}(\mathbf{x}). \quad (2.55)$$

The half time step in this equation shows that (2.51–2.54) is a leap-frog scheme, where the dual wave is evaluated at the time instants $(j + 1/2)\tau$, and the primary wave is evaluated at the time instants $j\tau$, for $j \geq 0$.

Similarly, we can use the first order system formulation of the ROM time stepping scheme (2.45–2.47) to define the dual ROM snapshots $\widehat{\mathbf{u}}_j^{\text{ROM}}$,

$$\frac{\mathbf{u}_{j+1}^{\text{ROM}} - \mathbf{u}_j^{\text{ROM}}}{\tau} = -\mathcal{L}^{\text{ROM}}(q)\widehat{\mathbf{u}}_j^{\text{ROM}}, \quad (2.56)$$

$$\frac{\widehat{\mathbf{u}}_j^{\text{ROM}} - \widehat{\mathbf{u}}_{j-1}^{\text{ROM}}}{\tau} = \mathcal{L}^{\text{ROM}}(q)^T \mathbf{u}_j^{\text{ROM}}, \quad j \geq 0, \quad (2.57)$$

$$\mathbf{u}_0^{\text{ROM}} = \mathbf{b}^{\text{ROM}} \quad (2.58)$$

$$\widehat{\mathbf{u}}_0^{\text{ROM}} + \widehat{\mathbf{u}}_{-1}^{\text{ROM}} = 0, \quad (2.59)$$

and obtain as above that

$$\widehat{\mathbf{u}}_0^{\text{ROM}} = \widehat{\mathbf{b}}^{\text{ROM}} = \frac{\tau}{2} \mathcal{L}^{\text{ROM}}(q)^T \mathbf{b}^{\text{ROM}}. \quad (2.60)$$

The orthogonalization of the dual snapshots and their use in the Galerkin-Petrov projection of $\mathcal{L}(q)$ are in the next theorem, proved in appendix D.

THEOREM 2.5. Denote by $\widehat{\mathbf{U}}(\mathbf{x}) = (\widehat{\mathbf{u}}_0(\mathbf{x}), \dots, \widehat{\mathbf{u}}_{n-1}(\mathbf{x}))$ the quasimatrix of the first n dual snapshots, which span the space $\widehat{\mathfrak{X}}$ defined in (2.50). The following statements hold:

(i) There exists an orthonormal basis of the space $\widehat{\mathfrak{X}}$, the columns of the quasimatrix $\widehat{\mathbf{V}}(\mathbf{x}) = (\widehat{\mathbf{v}}_0(\mathbf{x}), \dots, \widehat{\mathbf{v}}_{n-1}(\mathbf{x}))$, satisfying

$$\widehat{\mathbf{U}}(\mathbf{x}) = \widehat{\mathbf{V}}(\mathbf{x})\widehat{\mathbf{R}}, \quad (2.61)$$

where $\widehat{\mathbf{R}}$ is the matrix of the first n ROM dual snapshots

$$\widehat{\mathbf{R}} = (\widehat{\mathbf{u}}_0^{\text{ROM}}, \dots, \widehat{\mathbf{u}}_{n-1}^{\text{ROM}}). \quad (2.62)$$

This is the analogue of equations (2.31), (2.37), and $\widehat{\mathbf{R}}$ is block upper triangular.
(ii) The matrix $\mathcal{L}^{\text{ROM}}(q)$ defined in the Cholesky factorization (2.48) is the Galerkin-Petrov projection of the operator $\mathcal{L}(q)$ defined in (2.12), on the spaces \mathfrak{X} and $\widehat{\mathfrak{X}}$,

$$\mathcal{L}^{\text{ROM}}(q) = \mathbf{V}^T \mathcal{L}(q) \widehat{\mathbf{V}}. \quad (2.63)$$

Similar to Remark 2.2, we note that definition (2.61) of $\widehat{\mathbf{V}}(\mathbf{x})$ is the Gram-Schmidt orthogonalization of the dual snapshots, which gives the causal ROM dual snapshots gathered in the block upper triangular matrix $\widehat{\mathbf{R}}$.

2.5. Orthogonal transformations. The block Cholesky factorization (2.24) of the mass matrix is defined up to an orthogonal transformation of the form

$$\mathbf{Y} = \text{diag}(\mathbf{Y}_0, \dots, \mathbf{Y}_{n-1}), \quad (2.64)$$

with $m \times m$ orthogonal matrices \mathbf{Y}_j , for $j = 0, \dots, n-1$. That is to say, the matrix $\mathbf{Y}^T \mathbf{R}$ is also $nm \times nm$ block upper triangular, and satisfies

$$(\mathbf{Y}^T \mathbf{R})^T \mathbf{Y}^T \mathbf{R} = \mathbf{R}^T \mathbf{R} = \mathbf{M}. \quad (2.65)$$

Moreover, if we replace \mathbf{R} with $\mathbf{Y}^T \mathbf{R}$ in definitions (2.29–2.30), we get the ROM propagator

$$\mathbf{\Pi}^{\text{ROM}}(q) = \mathbf{Y}^T \mathcal{P}^{\text{ROM}}(q) \mathbf{Y}, \quad (2.66)$$

which has all the properties described in section 2.4. The quasimatrix of orthonormal snapshots is transformed to

$$\mathbf{V}(\mathbf{x}) = (\boldsymbol{\nu}_0(\mathbf{x}), \dots, \boldsymbol{\nu}_{n-1}(\mathbf{x})) = \mathbf{U}(\mathbf{x})(\mathbf{Y}^T \mathbf{R})^{-1} = \mathbf{V}(\mathbf{x}) \mathbf{Y}, \quad (2.67)$$

and for the dual snapshots we have, similarly,

$$\widehat{\mathbf{V}}(\mathbf{x}) = (\widehat{\boldsymbol{\nu}}_0(\mathbf{x}), \dots, \widehat{\boldsymbol{\nu}}_{n-1}(\mathbf{x})) = \widehat{\mathbf{V}}(\mathbf{x}) \widehat{\mathbf{Y}}. \quad (2.68)$$

The Galerkin-Petrov projection (2.63) becomes

$$\mathbf{\Lambda}^{\text{ROM}}(q) = \boldsymbol{\nu}^T \mathcal{L}(q) \widehat{\mathbf{V}} = \mathbf{Y}^T \mathcal{L}^{\text{ROM}}(q) \widehat{\mathbf{Y}}. \quad (2.69)$$

Here $\widehat{\mathbf{Y}}$ is another arbitrary orthogonal transformation of the form (2.64), and $\mathbf{\Lambda}^{\text{ROM}}(q)$ is block lower bidiagonal. In equations (2.66–2.69) we use greek letters for the transformed ROM and the orthonormal snapshots. These depend on \mathbf{Y} and $\widehat{\mathbf{Y}}$, but we suppress this dependence in the notation.

2.6. Connection to finite differences. To interpret the ROM matrix $\mathcal{L}^{\text{ROM}}(q)$ as an approximate finite difference scheme for the operator $L(q)$, we write it here explicitly using the following assumption:

ASSUMPTION 2.6. *The iteration*

$$[\varphi_{j+1}(\mathbf{x}) - \varphi_j(\mathbf{x})] \gamma_j^{-1} = -\mathcal{L}(q) \widehat{\varphi}_j(\mathbf{x}), \quad (2.70)$$

$$[\widehat{\varphi}_j(\mathbf{x}) - \widehat{\varphi}_{j-1}(\mathbf{x})] \widehat{\gamma}_j^{-1} = \mathcal{L}(q)^T \varphi_j(\mathbf{x}), \quad j \geq 0, \quad (2.71)$$

with initial conditions

$$\varphi_0(\mathbf{x}) = \mathbf{b}(\mathbf{x}), \quad \widehat{\varphi}_{-1}(\mathbf{x}) = \mathbf{0}, \quad (2.72)$$

and with $m \times m$ symmetric matrix coefficients

$$\widehat{\gamma}_j = \langle \varphi_j, \varphi_j \rangle^{-1}, \quad \gamma_j = \langle \widehat{\varphi}_j, \widehat{\varphi}_j \rangle^{-1}, \quad (2.73)$$

does not break down for $j = 0, \dots, n-1$. That is to say, the columns in each $\varphi_j(\mathbf{x})$ and $\widehat{\varphi}_j(\mathbf{x})$ remain linearly independent, so the matrices (2.73) are defined.

We explain in appendix E that this assumption is basically the same as saying that the first-order block Lanczos procedure (2.70)–(2.73) for calculating orthogonal bases of the spaces \mathfrak{X} and $\widehat{\mathfrak{X}}$ does not break down. If this is the case, we have the following result, proved in appendix E.

THEOREM 2.7. *Under the Assumption 2.6, there exists a choice of the square roots of the coefficients (2.73),*

$$\gamma_j = \mathbf{\Gamma}_j \mathbf{\Gamma}_j^T, \quad \widehat{\gamma}_j = \widehat{\mathbf{\Gamma}}_j \widehat{\mathbf{\Gamma}}_j^T, \quad j \geq 0, \quad (2.74)$$

which relates the orthonormal snapshots defined in (2.31) and (2.61) to the solution of the iteration (2.70–2.72) as follows,

$$\mathbf{v}_j(\mathbf{x}) = \varphi_j(\mathbf{x}) \widehat{\mathbf{\Gamma}}_j, \quad \widehat{\mathbf{v}}_j(\mathbf{x}) = \widehat{\varphi}_j(\mathbf{x}) \mathbf{\Gamma}_j, \quad j = 0, \dots, n-1. \quad (2.75)$$

Moreover, the block entries of the ROM matrix $\mathcal{L}^{\text{ROM}}(q)$ are defined by these square roots as

$$\mathcal{L}_{j,j}^{\text{ROM}}(q) = \widehat{\mathbf{\Gamma}}_j^{-1} \mathbf{\Gamma}_j^{-T}, \quad j = 0, \dots, n-1, \quad (2.76)$$

$$\mathcal{L}_{j+1,j}^{\text{ROM}}(q) = -\widehat{\mathbf{\Gamma}}_{j+1}^{-1} \mathbf{\Gamma}_j^{-T}, \quad j = 0, \dots, n-2. \quad (2.77)$$

Recall from section 2.1 that $\mathcal{L}(q)$ is an approximation of the first order partial differential operator $L(q)$. Equation (2.70) shows that this operator is captured by the ROM as a finite difference scheme, where each step corresponds to a time instant indexed by $j \geq 0$. The "steps" are $m \times m$ matrices, due to the fact that there are m source excitations. As the time index increases, the iteration (2.70–2.72) and definition (2.75) generate orthonormal snapshots that satisfy the causality relations (2.36) and (2.61). Initially, these snapshots are in the range of $\mathbf{u}_0(\mathbf{x}) = \mathbf{b}(\mathbf{x})$ and $\widehat{\mathbf{u}}_0(\mathbf{x}) = \widehat{\mathbf{b}}(\mathbf{x})$, respectively, and are supported near the array. At the next time instant the wave front advances to a depth of the order $c_o \tau$, so $\mathbf{u}_1(\mathbf{x})$ will have large entries around depth $c_o \tau$. Due to causality and orthogonality, $\mathbf{v}_1(\mathbf{x})$ should peak around this depth. The same holds for the dual orthonormal snapshots. Arguing this way, we expect that the peak values of the orthonormal snapshots follow the progression of the wave front inside the medium. This is confirmed by numerical simulations in [5, 6, 14].

REMARK 2.8. Every ROM matrix $\mathbf{\Lambda}^{\text{ROM}}(q)$ related to $\mathcal{L}^{\text{ROM}}(q)$ by (2.69) has the finite differences interpretation (2.70–2.72), (2.76–2.77), and it is the Galerkin-Petrov projection of the operator $\mathcal{L}(q)$ in the orthonormal bases

$$\boldsymbol{\nu}_j(\mathbf{x}) = \mathbf{v}_j(\mathbf{x})\mathbf{Y}_j = \boldsymbol{\varphi}_j(\mathbf{x})\widehat{\boldsymbol{\Gamma}}_j\mathbf{Y}_j, \quad \widehat{\boldsymbol{\nu}}_j(\mathbf{x}) = \widehat{\mathbf{v}}_j(\mathbf{x})\widehat{\mathbf{Y}}_j = \widehat{\boldsymbol{\varphi}}_j(\mathbf{x})\boldsymbol{\Gamma}_j\widehat{\mathbf{Y}}_j, \quad j \geq 0.$$

This non-uniqueness is due to the multiple choices of the square roots of $\boldsymbol{\gamma}_j$ and $\widehat{\boldsymbol{\gamma}}_j$,

$$\begin{aligned} \boldsymbol{\gamma}_j &= \boldsymbol{\Gamma}_j\boldsymbol{\Gamma}_j^T = (\boldsymbol{\Gamma}_j\widehat{\mathbf{Y}}_j)(\boldsymbol{\Gamma}_j\widehat{\mathbf{Y}}_j)^T, \\ \widehat{\boldsymbol{\gamma}}_j &= \widehat{\boldsymbol{\Gamma}}_j\widehat{\boldsymbol{\Gamma}}_j^T = (\widehat{\boldsymbol{\Gamma}}_j\mathbf{Y}_j)(\widehat{\boldsymbol{\Gamma}}_j\mathbf{Y}_j)^T, \quad j \geq 0. \end{aligned}$$

The block entries of $\mathbf{\Lambda}^{\text{ROM}}(q)$ are given by

$$\begin{aligned} \mathbf{\Lambda}_{j,j}^{\text{ROM}}(q) &= \mathbf{Y}_j^{-1}\widehat{\boldsymbol{\Gamma}}_j^{-1}\boldsymbol{\Gamma}_j^{-T}\widehat{\mathbf{Y}}_j^{-T} = \mathbf{Y}_j^T\mathcal{L}_{j,j}^{\text{ROM}}(q)\widehat{\mathbf{Y}}_j, \quad j = 0, \dots, n-1, \\ \mathbf{\Lambda}_{j+1,j}^{\text{ROM}}(q) &= -\mathbf{Y}_{j+1}^{-1}\widehat{\boldsymbol{\Gamma}}_{j+1}^{-1}\boldsymbol{\Gamma}_j^{-T}\widehat{\mathbf{Y}}_j^{-T} = \mathbf{Y}_{j+1}^T\mathcal{L}_{j+1,j}^{\text{ROM}}(q)\widehat{\mathbf{Y}}_j, \quad j = 0, \dots, n-2, \end{aligned}$$

which is precisely (2.69) written block-wise.

Assumption 2.6 and Theorem 2.7 are written as if we knew the operator $\mathcal{L}(q)$, which is not the case in the inverse problem. Their purpose is to interpret the ROM as a finite difference scheme, which we use in the next section to motivate the new inversion method. However, matrices $\{\boldsymbol{\gamma}_j, \widehat{\boldsymbol{\gamma}}_j\}_{0 \leq j \leq n-1}$ can be determined from the data, from the equation

$$\mathbf{Y}^T \frac{2}{\tau^2} \left(\mathbf{I}_{nm} - \mathcal{P}^{\text{ROM}}(q) \right) \mathbf{Y} = \mathbf{\Lambda}^{\text{ROM}}(q) \mathbf{\Lambda}^{\text{ROM}}(q)^T.$$

Substituting the expression of $\mathbf{\Lambda}^{\text{ROM}}(q)$ described in Remark 2.8, for a given convention of the matrix square root, and equating block-wise, one obtains an iteration which defines sequentially $\boldsymbol{\gamma}_j, \widehat{\boldsymbol{\gamma}}_j$, starting with $\widehat{\boldsymbol{\gamma}}_0 = \langle \mathbf{b}, \mathbf{b} \rangle^{-1}$, and also the diagonal blocks of \mathbf{Y} .

3. Inverse scattering. We now use the ROM for solving the inverse problem. The proposed method generalizes to all linear waves in isotropic media, in the backscattering setup described in the introduction. Nevertheless, to make the presentation explicit, we focus attention on inverse scattering for sound waves.

We refer to [5, 6] for the derivation of the hyperbolic problem (1.1–1.3) from the acoustic wave equation, where $\mathbf{u}(t, \mathbf{x})$ is related to the pressure and the operators $L(q)$ and $L(q)^T$ are given by

$$\begin{aligned} L(q)\widehat{\mathbf{u}}(t, \mathbf{x}) &= L(0)\widehat{\mathbf{u}}(t, \mathbf{x}) + \frac{1}{2}[c(\mathbf{x})\nabla q(\mathbf{x})] \cdot \widehat{\mathbf{u}}(t, \mathbf{x}), \\ L(q)^T\mathbf{u}(t, \mathbf{x}) &= L(0)^T\mathbf{u}(t, \mathbf{x}) + \frac{1}{2}[c(\mathbf{x})\nabla q(\mathbf{x})]\mathbf{u}(t, \mathbf{x}), \end{aligned} \quad (3.1)$$

with

$$\begin{aligned} L(0)\widehat{\mathbf{u}}(t, \mathbf{x}) &= -\sqrt{c(\mathbf{x})} \operatorname{div} [\sqrt{c(\mathbf{x})}\widehat{\mathbf{u}}(t, \mathbf{x})], \\ L(0)^T\mathbf{u}(t, \mathbf{x}) &= \sqrt{c(\mathbf{x})} \nabla [\sqrt{c(\mathbf{x})}\mathbf{u}(t, \mathbf{x})]. \end{aligned} \quad (3.2)$$

The dot in (3.1) denotes the inner product in \mathbb{R}^d and the vector-valued function $\widehat{\mathbf{u}}(t, \mathbf{x})$ is related to the acoustic velocity as in [5, 6].

Here $c(\mathbf{x})$ is the assumed smooth wave speed, the known kinematic model, and the unknown reflectivity is defined by

$$q(\mathbf{x}) = \ln \sqrt{\sigma(\mathbf{x})}, \quad (3.3)$$

in terms of the acoustic impedance $\sigma(\mathbf{x})$. As explained in the introduction, the model (3.1–3.3) arises when separating the estimations of the kinematic model (assumed known here) and the reflectivity. It applies to the backscattering setup, where as shown in [2], the reflections recorded at a small array are due mainly to relative variations of the impedance.

The main idea of our inversion method is that instead of using the conventional nonlinear least squares data fit minimization formulation, it is better to minimize the difference of the ROM matrices $\mathcal{L}^{\text{ROM}}(q) - \mathcal{L}^{\text{ROM}}(0)$, where $\mathcal{L}^{\text{ROM}}(0)$ is defined as in (2.48), but for the reference medium with zero reflectivity. We motivate this optimization formulation in section 3.1, with a discussion based on the results in sections 2.4–2.6. The inversion algorithm is described in section 3.2.

3.1. ROM parametrization of the reflectivity. There are two ways of understanding how the ROM encodes information about the unknown reflectivity (3.3). The first is based on the finite difference interpretation described in Theorem 2.7. The second is based on the Gram-Schmidt orthogonalization of the snapshots.

3.1.1. Finite differences interpretation. We see from definition (3.1) that the operator $L(q) - L(0)$ depends linearly on $q(\mathbf{x})$. Here we explain why the ROM version of this operator, the matrix $\mathcal{L}^{\text{ROM}}(q) - \mathcal{L}^{\text{ROM}}(0)$, is expected to inherit approximately this linear dependence.

Let us use Theorem 2.7 for the reference medium with zero reflectivity. We obtain the analogue of the finite difference scheme (2.70–2.72),

$$[\varphi_{j+1}^{(0)}(\mathbf{x}) - \varphi_j^{(0)}(\mathbf{x})] \mathbf{h}_j^{-1} = -\mathcal{L}(0) \widehat{\varphi}_j^{(0)}(\mathbf{x}), \quad (3.4)$$

$$[\widehat{\varphi}_j^{(0)}(\mathbf{x}) - \widehat{\varphi}_{j-1}^{(0)}(\mathbf{x})] \widehat{\mathbf{h}}_j^{-1} = \mathcal{L}(0)^T \varphi_j^{(0)}(\mathbf{x}), \quad j \geq 0, \quad (3.5)$$

$$\varphi_0^{(0)}(\mathbf{x}) = \varphi_0(\mathbf{x}) = \mathbf{b}(\mathbf{x}), \quad (3.6)$$

$$\widehat{\varphi}_{-1}^{(0)}(\mathbf{x}) = \widehat{\varphi}_{-1}(\mathbf{x}) = \mathbf{0}, \quad (3.7)$$

where the superscript (0) indicates that the reflectivity is zero, and the steps $\{\mathbf{h}_j, \widehat{\mathbf{h}}_j\}_{j \geq 0}$ are the analogues of (2.73),

$$\widehat{\mathbf{h}}_j = \langle \varphi_j^{(0)}, \varphi_j^{(0)} \rangle^{-1}, \quad \mathbf{h}_j = \langle \widehat{\varphi}_j^{(0)}, \widehat{\varphi}_j^{(0)} \rangle^{-1}, \quad j \geq 0. \quad (3.8)$$

The square roots of these steps

$$\mathbf{h}_j = \mathbf{H}_j \mathbf{H}_j^T, \quad \widehat{\mathbf{h}}_j = \widehat{\mathbf{H}}_j \widehat{\mathbf{H}}_j^T, \quad j \geq 0, \quad (3.9)$$

define the block lower bidiagonal ROM matrix $\mathcal{L}^{\text{ROM}}(0)$, with entries given by the analogues of (2.76–2.77),

$$\mathcal{L}_{j,j}^{\text{ROM}}(0) = \widehat{\mathbf{H}}_j^{-1} \mathbf{H}_j^{-T}, \quad j = 0, \dots, n-1, \quad (3.10)$$

$$\mathcal{L}_{j+1,j}^{\text{ROM}}(0) = -\widehat{\mathbf{H}}_{j+1}^{-1} \mathbf{H}_j^{-T}, \quad j = 0, \dots, n-2. \quad (3.11)$$

We now have two exact finite differences schemes: For the operator $\mathcal{L}^{\text{ROM}}(q)$, as given in (2.70–2.72), and for the operator $\mathcal{L}^{\text{ROM}}(0)$, as given in (3.4–3.7). To compare the two, let us use the transformation

$$\phi_j(\mathbf{x}) = \mathbf{v}_j(\mathbf{x}) \widehat{\mathbf{H}}_j^{-1} = \varphi_j(\mathbf{x}) \widehat{\Gamma}_j \widehat{\mathbf{H}}_j^{-1}, \quad (3.12)$$

$$\widehat{\phi}_j(\mathbf{x}) = \widehat{\mathbf{v}}_j(\mathbf{x}) \mathbf{H}_j^{-1} = \widehat{\varphi}_j(\mathbf{x}) \Gamma_j \mathbf{H}_j^{-1}, \quad j \geq 0, \quad (3.13)$$

so that $\phi_j(\mathbf{x})$ and $\widehat{\phi}_j(\mathbf{x})$ are normalized as in (3.8)

$$\langle \phi_j, \phi_j \rangle = \langle \varphi_j^{(0)}, \varphi_j^{(0)} \rangle = \widehat{\mathbf{h}}_j^{-1}, \quad \langle \widehat{\phi}_j, \widehat{\phi}_j \rangle = \langle \widehat{\varphi}_j^{(0)}, \widehat{\varphi}_j^{(0)} \rangle = \mathbf{h}_j^{-1}, \quad j \geq 0.$$

We also introduce the matrices

$$\sigma_j^{\frac{1}{2}} = \widehat{\Gamma}_j \widehat{\mathbf{H}}_j^{-1}, \quad \widehat{\sigma}_j^{\frac{1}{2}} = \mathbf{H}_j \Gamma_j^{-1}, \quad j \geq 0, \quad (3.14)$$

which will be interpreted below as approximations of the square root of the impedance. Substituting (3.12–3.13) in (2.70) and using definition (3.14), we obtain

$$\mathcal{L}(q) \widehat{\phi}_j(\mathbf{x}) + [\phi_{j+1}(\mathbf{x}) - \phi_j(\mathbf{x})] \mathbf{h}_j^{-1} = \phi_{j+1}(\mathbf{x}) \mathbf{Q}_j^+ + \phi_j(\mathbf{x}) \mathbf{Q}_j^-, \quad (3.15)$$

where the matrices

$$\mathbf{Q}_j^+ = \sigma_{j+1}^{-\frac{1}{2}} [\sigma_{j+1}^{\frac{1}{2}} - (\widehat{\sigma}_j^{\frac{1}{2}})^T] \mathbf{h}_j^{-1}, \quad \mathbf{Q}_j^- = \sigma_j^{-\frac{1}{2}} [(\widehat{\sigma}_j^{\frac{1}{2}})^T - \sigma_j^{\frac{1}{2}}] \mathbf{h}_j^{-1}, \quad (3.16)$$

satisfy

$$\sigma_{j+1}^{\frac{1}{2}} \mathbf{Q}_j^+ + \sigma_j^{\frac{1}{2}} \mathbf{Q}_j^- = [\sigma_{j+1}^{\frac{1}{2}} - \sigma_j^{\frac{1}{2}}] \mathbf{h}_j^{-1}. \quad (3.17)$$

The second term in the left hand side in (3.15) looks like the finite differences approximation of $-\mathcal{L}(0)$ in equation (3.4), although there the operator acts on a different space, spanned by the snapshots in the reference medium. The right hand side in (3.15) looks like a finite difference approximation of the operator

$$L(q) - L(0) \stackrel{(3.1)}{=} c(\mathbf{x}) \nabla q(\mathbf{x}) \cdot, \quad q(\mathbf{x}) = \ln \sqrt{\sigma(\mathbf{x})}.$$

The discretization corresponds to time stepping, so we can view \mathbf{h}_j and $\widehat{\mathbf{h}}_j$ as primary and dual grid steps for discretization in range. These steps depend on the kinematic model $c(\mathbf{x})$ which is the same in the reference and the unknown medium. The matrices $\sigma_j^{\frac{1}{2}}$ and $\widehat{\sigma}_j^{\frac{1}{2}}$ can be viewed as approximations of $\sqrt{\sigma(x)}$ on the primary grid and dual grid, respectively, and the matrices (3.16) can be viewed as approximations of $c(\mathbf{x}) \nabla q(\mathbf{x}) \cdot$, up to some factors which add up as in (3.17).

It remains to study the difference of the block lower bidiagonal ROM matrices $\mathcal{L}_{j,j}^{\text{ROM}}(q)$ and $\mathcal{L}_{j,j}^{\text{ROM}}(0)$, using the expressions (2.76–2.77) and (3.10–3.11) of their entries. We obtain that

$$\begin{aligned} \mathcal{L}_{j,j}^{\text{ROM}}(q) - \mathcal{L}_{j,j}^{\text{ROM}}(0) &= \widehat{\Gamma}_j^{-1} \Gamma_j^{-T} - \widehat{\mathbf{H}}_j^{-1} \mathbf{H}_j^{-T} \stackrel{(3.14)}{=} \widehat{\mathbf{H}}_j^{-1} \sigma_j^{-\frac{1}{2}} [(\widehat{\sigma}_j^{\frac{1}{2}})^T - \sigma_j^{\frac{1}{2}}] \mathbf{H}_j^{-T} \\ &\stackrel{(3.16)}{=} \widehat{\mathbf{H}}_j^{-1} \mathbf{Q}_j^- \mathbf{H}_j, \quad j = 0, \dots, n-1, \end{aligned} \quad (3.18)$$

and

$$\begin{aligned} \mathcal{L}_{j+1,j}^{\text{ROM}}(q) - \mathcal{L}_{j+1,j}^{\text{ROM}}(0) &= \widehat{\mathbf{H}}_{j+1}^{-1} \mathbf{H}_j^{-T} - \widehat{\Gamma}_{j+1}^{-1} \Gamma_j^{-T} \stackrel{(3.14)}{=} \widehat{\mathbf{H}}_{j+1}^{-1} \sigma_{j+1}^{-\frac{1}{2}} [\sigma_{j+1}^{\frac{1}{2}} - (\widehat{\sigma}_j^{\frac{1}{2}})^T] \mathbf{H}_j^{-T} \\ &\stackrel{(3.16)}{=} \widehat{\mathbf{H}}_{j+1}^{-1} \mathbf{Q}_j^+ \mathbf{H}_j, \quad j = 0, \dots, n-2. \end{aligned} \quad (3.19)$$

Therefore, $\mathcal{L}^{\text{ROM}}(q) - \mathcal{L}^{\text{ROM}}(0)$ is linear in the matrices \mathbf{Q}_j^\pm defined in (3.16), which are expected to approximate the gradient of the reflectivity, as explained above.

We remark that the approximate linear dependence of $L(q) - L(0)$ and therefore of $\mathcal{L}^{\text{ROM}}(q) - \mathcal{L}^{\text{ROM}}(0)$ on the gradient of the reflectivity is important in inversion, as it leads to an emphasis of the boundaries of reflectors and to sharp estimates of their support, as observed in the numerical results in section 4.

3.1.2. Gram-Schmidt orthogonalization interpretation. Recall Remark 2.2 on the causal construction of the orthonormal snapshots, via the Gram-Schmidt orthogonalization (2.31), and the similar result in section 2.4.3 for the orthonormal dual snapshots. We now explain that this construction leads to projection matrices $\mathbf{V}(\mathbf{x})$ and $\widehat{\mathbf{V}}(\mathbf{x})$ should be nearly independent of the unknown reflectivity. In light of Theorem 2.5, this implies that $\mathcal{L}^{\text{ROM}}(q)$ has approximately the same affine dependence on $q(\mathbf{x})$ as $L(q) \approx \mathcal{L}(q)$, and gives another motivation for the inversion based on $\mathcal{L}^{\text{ROM}}(q) - \mathcal{L}^{\text{ROM}}(0)$.

For simplicity of the argument, we assume in this section only that the kinematic model is constant $c(\mathbf{x}) = c_o$. The extension to arbitrary $c(x)$ is straightforward in one dimension, where we can use the travel time transformation $x \mapsto \int_0^x ds c^{-1}(s)$ to eliminate the wave speed from the wave equation. In higher dimensions the extension is not easy and may not even be true, unless the medium is nice enough, so that the wave progresses forward at each time step and there are no lensing effects, as we have assumed so far.

One dimension: We begin with the case $d = 1$, where the domain Ω is an interval. This is easier to understand because there is only one sensor ($m = 1$) and there are no block linear algebra calculations.

The Gram-Schmidt orthogonalization (2.31) is

$$\left(u_0(x), \dots, u_{n-1}(x) \right) = \left(v_0(x), \dots, v_{n-1}(x) \right) \mathbf{R}, \quad x \in \Omega, \quad (3.20)$$

where now \mathbf{R} is $n \times n$ upper triangular and we do not use bold symbols because the snapshots and x are real valued. Let us evaluate this equation at the locations $x_j = c_o j \tau$ of the wavefront at the first n time instants $j\tau$ of the measurements, for $j = 0, \dots, n-1$, and gather the results in the linear system

$$\begin{pmatrix} u_0(x_0) & \dots & u_{n-1}(x_0) \\ u_0(x_1) & \dots & u_{n-1}(x_1) \\ \vdots & & \vdots \\ u_0(x_{n-1}) & \dots & u_{n-1}(x_{n-1}) \end{pmatrix} = \begin{pmatrix} v_0(x_0) & \dots & v_{n-1}(x_0) \\ v_0(x_1) & \dots & v_{n-1}(x_1) \\ \vdots & & \vdots \\ v_0(x_{n-1}) & \dots & v_{n-1}(x_{n-1}) \end{pmatrix} \mathbf{R}. \quad (3.21)$$

The first factor in the right hand side is a nearly orthogonal matrix, because

$$\sum_{l=0}^{n-1} v_l(x_i) v_l(x_j) \approx \frac{1}{c_o \tau} \int_{\Omega} dx v_l(x) v_l(x) = \frac{1}{c_o \tau} \delta_{ij}, \quad i, j = 0, \dots, n-1. \quad (3.22)$$

Here the integral is approximated by a Riemann sum and the integrand is supported in the interval $[0, \min\{x_i, x_j\}] \subseteq [0, x_{n-1}] \subset \Omega$, by the causality relation (2.36).

We conclude that (3.21) is basically a QR factorization [15, Section 5.2], which seeks an orthonormal basis that transforms the left hand side to upper triangular form. But the left hand side is already upper triangular by construction

$$u_j(x) = 0 \text{ for } x > x_j, \quad j = 0, \dots, n-1,$$

so there is no transformation to be made, and

$$\begin{pmatrix} v_0(x_0) & \dots & v_{n-1}(x_0) \\ v_0(x_1) & \dots & v_{n-1}(x_1) \\ \vdots & & \vdots \\ v_0(x_{n-1}) & \dots & v_{n-1}(x_{n-1}) \end{pmatrix} \approx \frac{1}{\sqrt{c_o \tau}} \mathbf{I}_n, \quad (3.23)$$

up to \pm sign ambiguity on the diagonal. This matrix has exactly zero entries below the diagonal, by the causality of the orthonormal snapshots, so the approximation applies only to the upper triangular part. The quasimatrix $\mathbf{V}(x)$ of the orthonormal snapshots is an interpolation of the entries in (3.23), so it is approximately independent of $q(x)$. The same argument applies to the quasimatrix $\widehat{\mathbf{V}}(x)$ of orthonormal dual snapshots.

REMARK 3.1. We expect from (3.22–3.23) that the approximation of the quasimatrix $\mathbf{V}(x)$ and its dual analogue $\widehat{\mathbf{V}}(x)$ by a multiple of the identity improves when we decrease the time sampling interval τ . This is the case up to a point, because if τ is too small, then the snapshots become linearly dependent (up to machine precision) and the mass matrix (2.21) is no longer invertible. A good strategy for choosing τ is according to the Nyquist criterion which takes into consideration the temporal period of oscillation of the wave.

Higher dimensions: Here we have the block Gram-Schmidt orthogonalization

$$\left(\mathbf{u}_0(\mathbf{x}), \dots, \mathbf{u}_{n-1}(\mathbf{x})\right) = \left(\mathbf{v}_0(x), \dots, \mathbf{v}_{n-1}(x)\right) \mathbf{R}, \quad \mathbf{x} \in \Omega, \quad (3.24)$$

where \mathbf{R} is $nm \times nm$ block upper triangular, with $m \times m$ blocks.

To write equation (3.24) as a block QR factorization, the analogue of (3.21), consider the system of coordinates $\mathbf{x} = (x, \mathbf{x}^\perp) \in \Omega$, with origin at the center of the array, where $x \in [0, x_{\max}]$ is the depth (range) coordinate orthogonal to the array and \mathbf{x}^\perp is the cross-range in the plane of the array. Then, we can evaluate (3.24) at points

$$(x_j, \mathbf{x}_s^\perp), \quad x_j = c_o j \tau, \quad j = 0, \dots, n-1, \quad s = 1, \dots, m,$$

for some appropriate $\{\mathbf{x}_s^\perp\}_{1 \leq s \leq m}$. Using the block notation

$$\underline{\mathbf{u}}_j(x) = \begin{pmatrix} \mathbf{u}_j(x, \mathbf{x}_1^\perp) \\ \vdots \\ \mathbf{u}_j(x, \mathbf{x}_m^\perp) \end{pmatrix} \in \mathbb{R}^{m \times m}, \quad \underline{\mathbf{v}}_j(x) = \begin{pmatrix} \mathbf{v}_j(x, \mathbf{x}_1^\perp) \\ \vdots \\ \mathbf{v}_j(x, \mathbf{x}_m^\perp) \end{pmatrix} \in \mathbb{R}^{m \times m}, \quad (3.25)$$

we get

$$\begin{pmatrix} \underline{\mathbf{u}}_0(x_0) & \dots & \underline{\mathbf{u}}_{n-1}(x_0) \\ \underline{\mathbf{u}}_0(x_1) & \dots & \underline{\mathbf{u}}_{n-1}(x_1) \\ \vdots & & \vdots \\ \underline{\mathbf{u}}_0(x_{n-1}) & \dots & \underline{\mathbf{u}}_{n-1}(x_{n-1}) \end{pmatrix} = \begin{pmatrix} \underline{\mathbf{v}}_0(x_0) & \dots & \underline{\mathbf{v}}_{n-1}(x_0) \\ \underline{\mathbf{v}}_0(x_1) & \dots & \underline{\mathbf{v}}_{n-1}(x_1) \\ \vdots & & \vdots \\ \underline{\mathbf{v}}_0(x_{n-1}) & \dots & \underline{\mathbf{v}}_{n-1}(x_{n-1}) \end{pmatrix} \mathbf{R}. \quad (3.26)$$

Again, by construction,

$$\underline{\mathbf{u}}_j(x) = \mathbf{0}, \quad x > c_o j \tau,$$

so the left hand side in (3.26) is block upper triangular. The products of the block columns in the right hand side are, similar to the one-dimensional case,

$$\sum_{l=0}^{n-1} \underline{\mathbf{v}}_l(x_l)^T \underline{\mathbf{v}}_j(x_l) \approx \frac{1}{c_o \tau} \int_0^{x_{\max}} dx \underline{\mathbf{v}}_l(x)^T \underline{\mathbf{v}}_j(x), \quad (3.27)$$

where the left hand side is a Riemann sum approximation of the integral and the integrand is supported in $[0, \min\{x_i, x_j\}] \subseteq [0, x_{n-1}] \subset \Omega$, by the causality relation (2.36). Writing

more explicitly (3.27),

$$\begin{aligned} \sum_{l=0}^{n-1} \underline{\mathbf{v}}_i(x_l)^T \underline{\mathbf{v}}_j(x_l) &\approx \frac{1}{c_o \tau} \int_0^{x_{\max}} dx \sum_{s=1}^m \mathbf{v}_i(x, \mathbf{x}_s^\perp)^T \mathbf{v}_j(x, \mathbf{x}_s^\perp) \\ &\approx K \int_{\Omega} d\mathbf{x} \mathbf{v}_i(\mathbf{x})^T \mathbf{v}_j(\mathbf{x}) = K \mathbf{I}_m, \end{aligned} \quad (3.28)$$

where $d\mathbf{x} = dx d\mathbf{x}^\perp$, K is a constant, and the accuracy of the last approximation depends on the points $\{\mathbf{x}_s^\perp\}_{1 \leq s \leq m}$ and on how the wave propagates. Intuitively, the points $\{\mathbf{x}_s^\perp\}_{1 \leq s \leq m}$ should be near the m sensors in the array, and the approximation (3.28) should hold at least if n is not too large, meaning that for $j = 0, \dots, n-1$, the wave $\mathbf{u}_j(\mathbf{x})$ has not spread out much in cross-range, but propagates downward like a beam.

If the approximation (3.28) holds, then we have the analogue of the result in one dimension, where (3.26) is the block QR factorization of the block upper triangular matrix in the left hand side and the first factor in the right hand side is a multiple of the identity. The quasimatrix $\mathbf{V}(\mathbf{x})$ is the interpolation of this matrix and is therefore approximately independent of $q(\mathbf{x})$. The approximate independence of the quasimatrix $\hat{\mathbf{V}}(\mathbf{x})$ on $q(\mathbf{x})$ follows similarly.

The numerical simulations in [6, 5, 14] confirm this statement, and they also show that the approximation deteriorates for larger n . This is why in our inversion method we do not rely on the assumption that $\mathcal{L}^{\text{ROM}}(q) - \mathcal{L}^{\text{ROM}}(0)$ is linear in the reflectivity, and formulate instead a nonlinear minimization problem that is solved iteratively.

3.2. Inversion method. The classic way of solving the inverse problem is to estimate $q(\mathbf{x})$ using least squares data fit optimization

$$q^{\text{LS}}(\mathbf{x}) = \arg \min_{q^S \in \mathcal{Q}} \sum_{j=0}^{2n-1} \|\mathbf{D}_j - \langle \mathbf{b}, \mathcal{T}_j(\mathcal{P}(q^S)) \mathbf{b} \rangle\|_F^2, \quad (3.29)$$

where $\|\cdot\|_F$ denotes the Frobenius norm and we used equations (1.5) and (2.8) to write the mapping of the guess reflectivity q^S to the data. The search space is

$$\mathcal{Q} = \text{span}\{\psi_1(\mathbf{x}), \dots, \psi_{N^S}(\mathbf{x})\}, \quad (3.30)$$

for some carefully chosen basis functions $\{\psi_j(\mathbf{x})\}_{1 \leq j \leq N^S}$, with $\mathbf{x} \in \Omega$. Problem (3.29) is clearly nonlinear, and depending on the space (3.30) the Jacobian of the mapping

$$q^S \mapsto \{\langle \mathbf{b}, \mathcal{T}_j(\mathcal{P}(q^S)) \mathbf{b} \rangle\}_{0 \leq j \leq 2n-1} \quad (3.31)$$

may be poorly conditioned, which means that (3.29) should be regularized. Following the geophysics literature [17, 12] we refer to the inversion procedure for solving (3.29) with a Gauss-Newton iteration as the least squares reverse time migration (LS-RTM).

In contrast to the conventional approach (3.29), we estimate the reflectivity by the solution of the minimization problem

$$q^*(\mathbf{x}) = \arg \min_{q^S \in \mathcal{Q}} \|\mathcal{L}^{\text{ROM}}(q) - \mathcal{L}^{\text{ROM}}(q^S)\|_F^2, \quad (3.32)$$

because as discussed in the previous section, the matrix $\mathcal{L}^{\text{ROM}}(q) - \mathcal{L}^{\text{ROM}}(0)$ is expected to be approximately linear in $q(\mathbf{x})$. This is confirmed by the numerical results, which show that the Gauss-Newton iteration [18, Section 10.3] converges in a few steps. For the sake of brevity we refer to such iteration for solving (3.32) as ROM-GN. We emphasize that the construction of $\mathcal{L}^{\text{ROM}}(q)$ uses the data \mathbf{D}_j that depend non-linearly on the unknown reflectivity q .

3.2.1. Parametrization and resolution. For noisy data, regularization is needed in both the construction of the ROM (see [6]) and in the inversion. In the numerical simulations we regularize the Gauss-Newton method using a truncated SVD approach. But regardless of the noise, the basis functions of the sample space (3.29) should be defined based on a resolution study, to avoid over parametrizing the unknown reflectivity. This ensures that we have a well conditioned Jacobian and also saves computational time by limiting the dimension N^S of the search space \mathcal{Q} .

For the given excitation $\mathbf{b}(\mathbf{x})$, the resolution depends on the location in Ω , as we now explain. Let $\delta_j(\mathbf{x})$ be a non-negative function which integrates to one and has support centered at $\mathbf{x}_j \in \Omega$, of diameter $\lambda/2$, the Rayleigh resolution limit [7, Chapter VIII] for imaging with waves at central wavelength λ . We may think of δ_j as an approximate Dirac $\delta(\mathbf{x} - \mathbf{x}_j)$. From sections 2 and 3.1 we know that

$$\begin{aligned}\Delta \mathcal{L}^{\text{ROM}}(\delta_j) &\approx \mathbf{V}^{(0)T} \Delta \mathcal{L}(\delta_j) \widehat{\mathbf{V}}^{(0)} \approx \mathbf{V}^{(0)T} \Delta L(\delta_j) \widehat{\mathbf{V}}^{(0)} \stackrel{(3.1)}{\approx} \frac{c(\mathbf{x}_j)}{2} \mathbf{V}^{(0)T} \nabla \delta_j(\mathbf{x}) \cdot \widehat{\mathbf{V}}^{(0)}, \\ \Delta \mathcal{L}^{\text{ROM}}(\delta_j)^T &\approx \widehat{\mathbf{V}}^{(0)T} \Delta \mathcal{L}(\delta_j)^T \mathbf{V}^{(0)} \approx \widehat{\mathbf{V}}^{(0)T} \Delta L(\delta_j)^T \mathbf{V}^{(0)} \stackrel{(3.1)}{\approx} \frac{c(\mathbf{x}_j)}{2} \widehat{\mathbf{V}}^{(0)T} \nabla \delta_j(\mathbf{x}) \mathbf{V}^{(0)}.\end{aligned}$$

Here we denote $\Delta \mathcal{L}^{\text{ROM}}(\delta_j) = \mathcal{L}^{\text{ROM}}(\delta_j) - \mathcal{L}^{\text{ROM}}(0)$, $\Delta \mathcal{L}(\delta_j) = \mathcal{L}(\delta_j) - \mathcal{L}(0)$ and $\Delta L(\delta_j) = L(\delta_j) - L(0)$, and similarly for the adjoints $\Delta \mathcal{L}^{\text{ROM}}(\delta_j)^T$, $\Delta \mathcal{L}(\delta_j)^T$ and $\Delta L(\delta_j)^T$. The quasimatrices $\mathbf{V}^{(0)}(\mathbf{x})$ and $\widehat{\mathbf{V}}^{(0)}(\mathbf{x})$ contain the primary and dual orthonormal snapshots calculated in the known reference medium with zero reflectivity. The dot denotes the inner product in \mathbb{R}^d and is understood component-wise, i.e.,

$$\nabla \delta_j(\mathbf{x}) \cdot \widehat{\mathbf{V}}^{(0)}(\mathbf{x}) = (\nabla \delta_j(\mathbf{x}) \cdot \widehat{\mathbf{v}}_0^{(0)}(\mathbf{x}), \dots, \nabla \delta_j(\mathbf{x}) \cdot \widehat{\mathbf{v}}_{n-1}^{(0)}(\mathbf{x})).$$

Therefore, we have

$$\Delta \mathcal{L}^{\text{ROM}}(\delta_j) \Delta \mathcal{L}^{\text{ROM}}(\delta_j)^T \approx \frac{c^2(\mathbf{x}_j)}{4} \mathbf{V}^{(0)T} \nabla \delta_j(\mathbf{x}) \cdot \widehat{\mathbf{V}}^{(0)} \widehat{\mathbf{V}}^{(0)T} \nabla \delta_j(\mathbf{x}) \mathbf{V}^{(0)},$$

in the ROM space, and in the physical space we get

$$\mathbf{V}^{(0)} \Delta \mathcal{L}^{\text{ROM}}(\delta_j) \Delta \mathcal{L}^{\text{ROM}}(\delta_j)^T \mathbf{V}^{(0)T} \approx \frac{c^2(\mathbf{x}_j)}{4} \mathbb{P}^{(0)} \nabla \delta_j(\mathbf{x}) \cdot \widehat{\mathbb{P}}^{(0)} \nabla \delta_j(\mathbf{x}) \mathbb{P}^{(0)}. \quad (3.33)$$

Here $\mathbb{P}^{(0)} = \mathbf{V}^{(0)} \mathbf{V}^{(0)T}$ is the orthogonal projector on the space of the first n snapshots in the reference medium, which takes any $\varphi(\mathbf{x})$ in the space of the snapshots and returns

$$\mathbf{V}^{(0)} \mathbf{V}^{(0)T} \varphi(\mathbf{x}) = \sum_{j=0}^{n-1} \mathbf{v}_j^{(0)}(\mathbf{x}) \langle \mathbf{v}_j^{(0)}, \varphi \rangle. \quad (3.34)$$

Similarly, $\widehat{\mathbb{P}}^{(0)} = \widehat{\mathbf{V}}^{(0)} \widehat{\mathbf{V}}^{(0)T}$ is the orthogonal projector on the space of the first n dual snapshots in the reference medium.

Equation (3.33) is the ROM approximation of the operator in

$$\Delta L(\delta_j) \Delta L(\delta_j)^T \varphi(\mathbf{x}) = \frac{c^2(\mathbf{x})}{4} |\nabla \delta_j(\mathbf{x})|^2 \varphi(\mathbf{x}) \approx \frac{c^2(\mathbf{x}_j)}{4} |\nabla \delta_j(\mathbf{x})|^2 \varphi(\mathbf{x}), \quad (3.35)$$

which acts as point-wise multiplication. Therefore, we define the resolution (point spread) function at point \mathbf{x}_j by

$$\begin{aligned}\Psi_j(\mathbf{x}) &= \left[\mathbf{V}^{(0)}(\mathbf{x}) \Delta \mathcal{L}^{\text{ROM}}(\delta_j) \Delta \mathcal{L}^{\text{ROM}}(\delta_j)^T \mathbf{V}^{(0)T}(\mathbf{x}) \right]^{\frac{1}{2}} \\ &= \|\mathbf{V}^{(0)}(\mathbf{x}) \Delta \mathcal{L}^{\text{ROM}}(\delta_j)\|_2, \quad \mathbf{x} \in \Omega,\end{aligned} \quad (3.36)$$

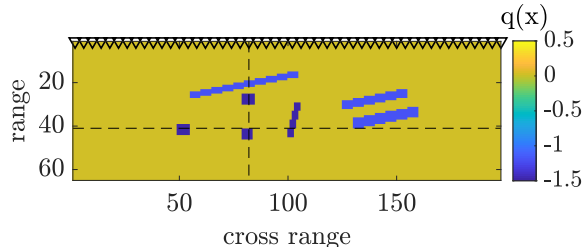


FIG. 4.1. Numerical experiment setup with sources and receivers depicted as ∇ . The dashed horizontal and vertical line are slices at which the inversion result is displayed in Fig. 4.6. The range and cross range are in units of ℓ . The reflectivity $q(\mathbf{x})$ is dimensionless by definition (3.3) and is supported at the scatterers shown in different shades of blue.

where $\|\cdot\|_2$ is the Euclidian norm in the space of row-vectors $\mathbb{R}^{1 \times nm}$.

We will see from the display of the point spread function (3.36) in the numerical section that its support grows with the distance (range) x_j of the point $\mathbf{x}_j = (x_j, \mathbf{x}_j^\perp)$. Moreover, the spreading is mostly in the cross-range direction, as expected from the classic resolution limits of imaging methods [7, Chapter VIII]. We choose the basis $\{\psi_j(\mathbf{x})\}_{1 \leq j \leq N^S}$ of the search space (3.30) as the continuous, piecewise linear (hat) functions on a mesh defined as follows: The discretization in range is determined by the range support of (3.36), which is basically unchanged throughout the domain if the background wave speed does not have large variations. Let N_r be the number of range points. Then, for any given range x_j , with $j = 1, \dots, N_r$, we discretize in cross-range at steps determined by the support of (3.36). This can be achieved for example by seeking an approximate partition of unity using the point spread function (3.36) in the range direction and the cross-range direction, respectively. The result is a non-uniform (deformed rectangular) mesh with N^S points, which we then triangularize to define the hat functions.

4. Numerical results. In this section we present two dimensional numerical results for configurations of scatterers modeled by the reflectivity in figures 4.1 and 4.7. All lengths are normalized by ℓ , the step size of the square mesh used to discretize the true medium in the time domain finite differences simulations for generating the synthetic data. The accessible boundary is modeled as sound hard and the inaccessible boundary as sound soft. Time is normalized by the sampling step τ . The initial wave $\mathbf{b}(\mathbf{x})$ is defined as in [6, Equation (95)] in terms of the pulse emitted by the sensors, which is a Ricker wavelet. The central wavelength calculated at the reference wave speed $c_o = 1.8\ell/\tau$ is $\lambda = 8.9\ell$ and the smallest wavelength, at 5% (i.e. -25dB) cut-off, is 4.5ℓ .

The first results, presented in section 4.1, are with noiseless data. The second set of results, in section 4.2, is for noisy data.

4.1. Inversion with noiseless data. In the first numerical experiment we seek to estimate the reflectivity displayed in Fig. 4.1. The kinematic model is constant

$$c(\mathbf{x}) = c_o = 1.8\ell/\tau,$$

and the array has $m = 50$ sensors separated by 4ℓ , displayed as triangles in the figure. The time sampling of the data is at interval τ chosen such that the smallest period of oscillation in the probing pulse, at 5% cut-off, equals 2.5τ . The data are collected at $2n = 110$ time steps, which leads to a data cube of dimension $110 \times 50 \times 50$.

We display in the left plot of Fig. 4.2 the point spread function defined in (3.36), for various points in the search region, shown with green dots. Note how its cross-range support

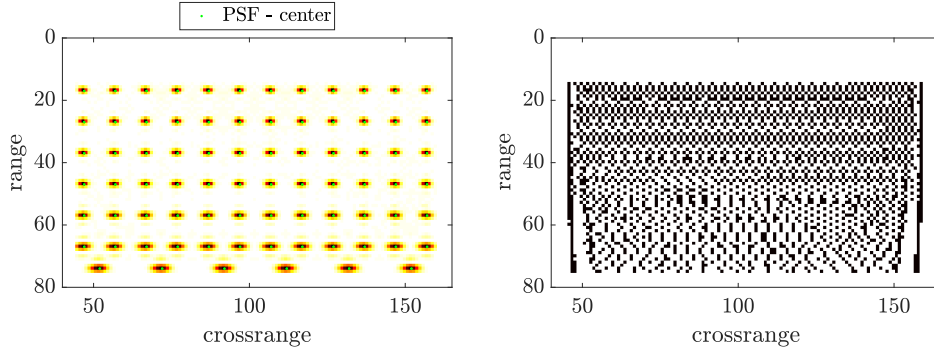


FIG. 4.2. Left: The point spread function (3.36) displayed at various range and cross range locations in the search region, for the setup in Fig. 4.1. Right: Centers of the point spread function selected from the partition of unity. The axes are in units of ℓ .

spreads deep inside the medium. The parametrization

$$q^S(\mathbf{x}) = \sum_{j=1}^{N^S} q_j^S \psi_j(\mathbf{x}), \quad (4.1)$$

of the guess reflectivity is given by the continuous piecewise linear hat functions $\psi_j(\mathbf{x})$ defined on the mesh shown in the right plot of Fig. 4.2. This mesh has the uniform spacing $c_0\tau$ in range and the points in the cross-range are calculated using an approximate partition of unity with the functions (3.36). That is to say, at any given range x_r , we solved the minimization problem

$$\min \|\boldsymbol{\alpha}\|_1, \quad \text{such that } \left| 1 - \sum_j \alpha_j \Psi(x_r, \mathbf{x}_j^\perp) \right| \leq \text{tolerance},$$

where $\boldsymbol{\alpha}$ is the vector of components α_j , the coefficients of the point spread function at the points in the search cross-range interval. Due to the loss of resolution with depth, we have fewer points deep in the domain. In this example we used the tolerance of 2%.

The data obtained with the excitation from the center sensor in the array are displayed in the left plot in Fig. 4.3. Note that to save computational time, we made the domain Ω smaller than assumed in the analysis. Therefore, the fictitious boundary $\partial\Omega_{\text{inac}}$ causes reflections that are visible at the bottom corners of the plot. In the right plot we display the data processed with [6, Algorithm 1], which is designed to return an approximation of the Born (single scattering) linear data model,

$$\mathbf{D}_j^{\text{Born}} = \mathbf{D}_j(0) + \mathbf{b}^{\text{ROM}T} \frac{d}{d\epsilon} \mathcal{T}_j(\mathcal{P}_\epsilon^{\text{ROM}}(q)) \Big|_{\epsilon=0} \mathbf{b}^{\text{ROM}}, \quad j = 0, \dots, 2n-1. \quad (4.2)$$

Here $\mathbf{D}_j(0)$ are the data simulated for the reference medium with no reflectivity and the right hand side is calculated using

$$\mathcal{P}_\epsilon^{\text{ROM}}(q) = \mathbf{I}_{nm} - \frac{\tau^2}{2} \mathcal{L}_\epsilon^{\text{ROM}}(q) \mathcal{L}_\epsilon^{\text{ROM}}(q)^T \approx \mathcal{P}^{\text{ROM}}(\epsilon q), \quad (4.3)$$

$$\mathcal{L}_\epsilon^{\text{ROM}}(q) = \mathcal{L}^{\text{ROM}}(0) + \epsilon (\mathcal{L}^{\text{ROM}}(q) - \mathcal{L}^{\text{ROM}}(0)) \approx \mathcal{L}^{\text{ROM}}(\epsilon q). \quad (4.4)$$

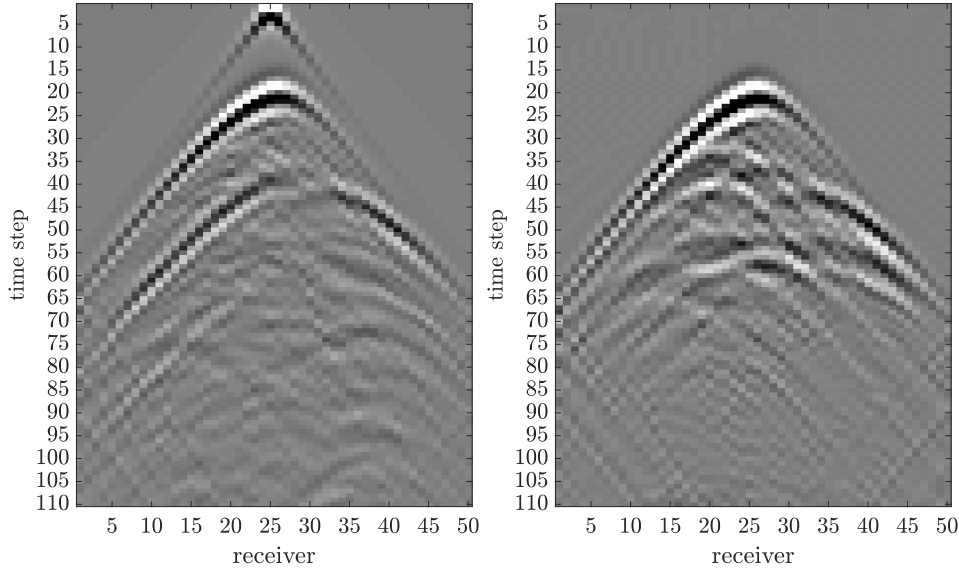


FIG. 4.3. The 25th column of \mathbf{D}_j (left plot) and of \mathbf{D}_j^{Born} (right plot), for $j = 0, \dots, 2n - 1$, as a function of time in the ordinate, in units of τ , and the receiver index in the abscissa.

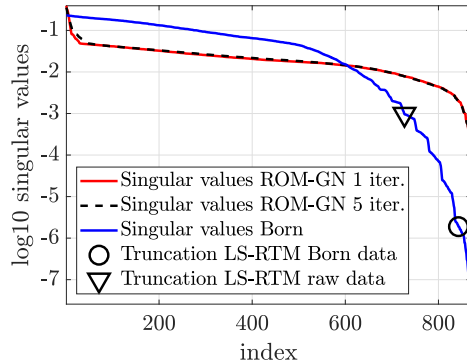


FIG. 4.4. Squared singular values of the Jacobian of the mapping $q^S \mapsto \{\mathbf{D}_j^{Born}\}_{0 \leq j \leq 2n-1}$ (blue curve) and of the mapping $q^S \mapsto \mathcal{L}^{ROM}(q^S)$ for the first and fifth Gauss-Newton iterates (red and black curves, respectively). The LS-RTM formulations with Born and raw data are regularized using truncated SVD at the values indicated with the circle and triangle, respectively.

We begin the comparison between the conventional LS-RTM and the proposed ROM-GN with a study of Jacobians of the corresponding mappings. As shown in Fig. 4.4, the Jacobian of $q \mapsto \{\mathbf{D}_j^{Born}\}_{0 \leq j \leq 2n-1}$ has worse conditioning compared to the Jacobian of $q \mapsto \mathcal{L}^{ROM}(q)$. Consequently, while LS-RTM required regularization via SVD truncation, we did not use regularization in ROM-GN ^{||}.

In Fig. 4.5 we compare the inversion results for both LS-RTM and ROM-GN approaches. For LS-RTM (top plots) we performed a single Gauss-Newton iteration using as input both the raw data $\{\mathbf{D}_j\}_{0 \leq j \leq 2n-1}$ (top left plot) and the processed (Born) data (4.2) (top right

^{||}However, we used the algorithm described in [6], based on a truncated SVD of the mass matrix, for the computation of the ROM and the transformation (4.2).

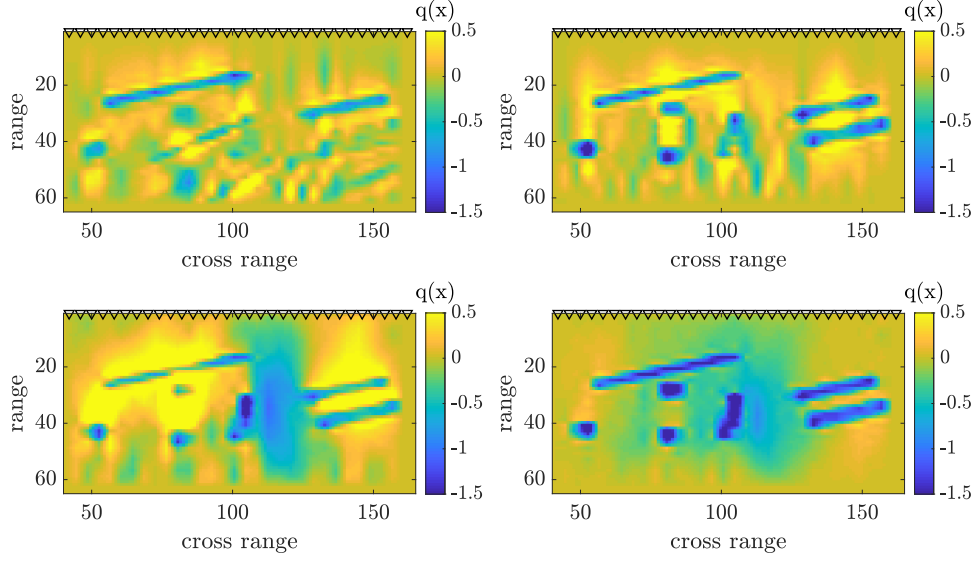


FIG. 4.5. Inversion results comparison. Top row: LS-RTM with raw data (left plot) and the transformed (Born) data (right plot). Bottom row: ROM-GN after 1 iteration (left plot) and 5 iterations (right plot). The axes are in units of ℓ .

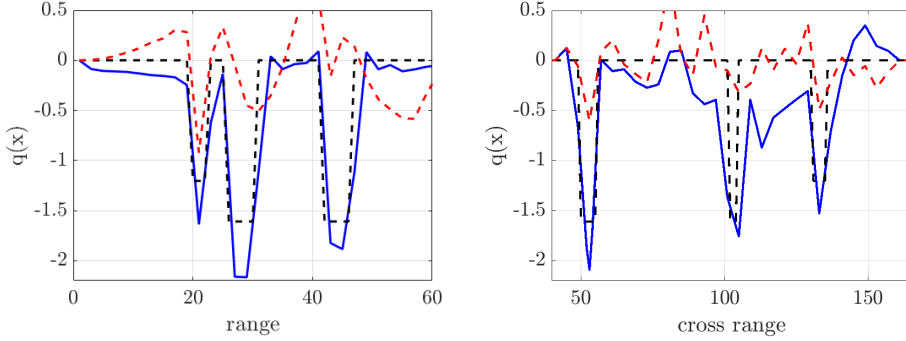


FIG. 4.6. Comparison of inversion results along the range (left plot) and cross range (right plot) slices taken at the lines shown in Fig. 4.1. The true reflectivity $q(x)$ is dashed black, LS-RTM inversion result is dashed red, ROM-GN inversion result is solid blue. The abscissa is in units of ℓ .

plot), which is intended to transform the problem into linear least squares. The image with the latter is better, as expected, because the multiple scattering effects have been removed approximately. Nevertheless, we observe image artifacts, due to the ill-conditioning of the Jacobian of the mapping $q \mapsto \{D_j^{Born}\}_{0 \leq j \leq 2n-1}$. In our experience, performing more Gauss-Newton iterations does not lead to an improved image, mostly because the transformed data (4.2) are a very good approximation of the linearized (Born) data.

The reflectivity obtained with ROM-GN is shown in the bottom two plots in Fig. 4.5 both after a single (bottom left plot) and five (bottom right plot) Gauss-Newton iterations, where convergence was achieved. Note that the shape of the scatterers is recovered well, because the operator (3.1) depends on the gradient of the reflectivity. Thus, it is easier to get the jumps of $q(x)$ than its smooth part. However, after five iterations the magnitudes of the scatterers are also recovered very well, as clearly seen in the range and cross range slice plots shown in

Fig. 4.6.

The ROM-GN uses the raw data $\{\mathbf{D}_j\}_{0 \leq j \leq 2n-1}$ and thus takes into account multiple scattering effects, which contain valuable information about the reflectivity q that may not be captured in $\{\mathbf{D}_j^{Born}\}_{0 \leq j \leq 2n-1}$. Thus, we observe a clear advantage of our ROM-GN approach at recovering both the shapes and magnitudes of scatterers compared to the conventional LS-RTM.

4.2. Inversion with noisy data. The second numerical experiment is motivated by the application of non-destructive testing, and seeks to estimate multiple fractures modeled by the reflectivity displayed in Fig. 4.7. The excitation is the same as in the previous experiment, except that the array has 32 sensors separated by 8ℓ and the kinematic model is no longer constant. The data are displayed in the left plot of Fig. 4.8 and are contaminated with 5% additive, white Gaussian noise. They are sampled at $2n = 170$ time steps, at interval τ calculated so that the smallest period of oscillation in the probing pulse, at 5% cut-off, equals 2τ . The transformed data (4.2) are displayed in the right plot of Fig. 4.8. We note in particular the multiple echo around time 90τ that is suppressed after the transformation.

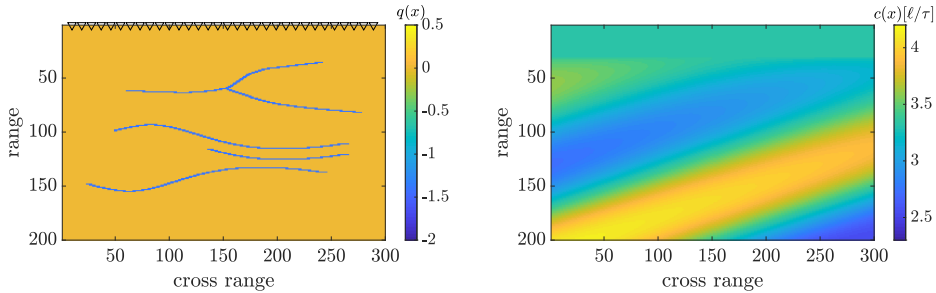


FIG. 4.7. Left: True reflectivity $q(x)$ modeling multiple fractures (thin regions with smaller acoustic impedance). Right: Kinematic model, with $c(x)$ displayed in units ℓ/τ . The array is shown on the top in the left plot. The axes are in units of ℓ .

We display in Fig. 4.9 the point spread function $\Psi_j(\mathbf{x})$ defined in (3.36), at different locations \mathbf{x}_j in the search domain, indicated by the dots. Note that the spread function looks different than in Fig. 4.2 due to the variable kinematic model. The mesh calculated as explained in the previous section is shown in the right plot in Fig. 4.9.

We compare the inversion results for LS-RTM and ROM-GN with noisy data in Fig. 4.10. We observe that the LS-RTM inversion results are better than in the previous experiment because the reflectivity contrast is not as strong. Nevertheless, even when given the transformed (Born) data (top right plot in Fig. 4.10), the LS-RTM does not recover the two bottom cracks very clearly. A much better inversion result is obtained with ROM-GN after five iterations which resolves all cracks, as shown in the bottom right plot in Fig. 4.10. Note that both LS-RTM and ROM-GN methods were regularized with a truncated SVD of the Jacobian.

5. Summary. We introduced a novel method for the inverse scattering problem, where the goal is to estimate reflective structures in a medium from data gathered by an active array of sensors. These sensors emit waves that propagate through the medium and measure the backscattered returns at $2n$ time instants separated by an appropriately chosen interval. The new algorithm is based on a reduced order model (ROM) of the wave propagator operator. This operator maps the wave from one time instant to the next, and is unknown in inverse scattering. However, the ROM can be calculated from the measurements at the array. We described the ROM for a generic hyperbolic system and showed that it corresponds to a Galerkin

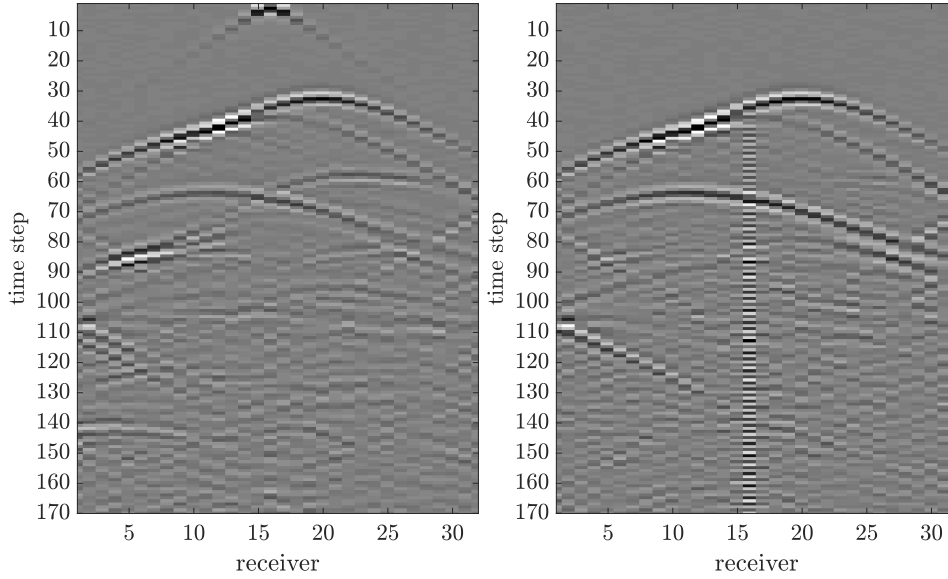


FIG. 4.8. The 16th columns of \mathbf{D}_j (left plot) and of \mathbf{D}_j^{Born} (right plot), for $j = 0, \dots, 2n - 1$, as a function of time in the ordinate, in units of τ , and the receiver index in the abscissa.

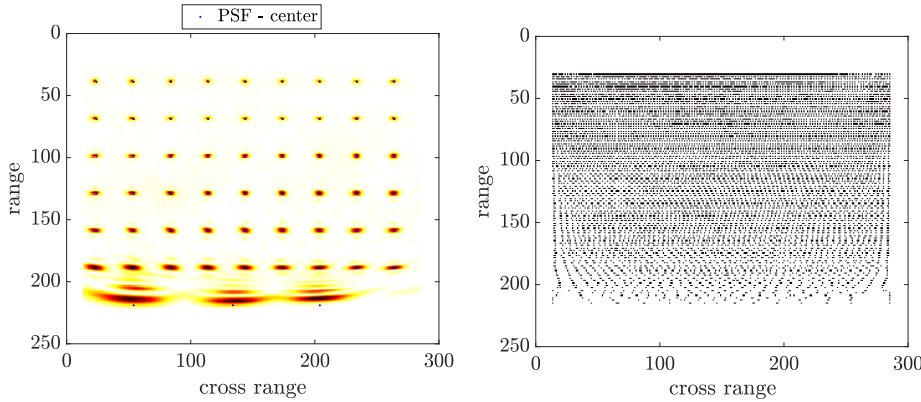


FIG. 4.9. Left: The point spread function (3.36) displayed at various range and cross range locations in the search region, for the setup in Fig. 4.7. Right: Centers of the point spread function selected from the partition of unity. The axes are in units of ℓ .

projection of the propagator operator on the space spanned by the wave at the first n times instants. We analyzed the ROM in the Galerkin framework, and used the results to motivate the new inversion method. We described the implementation of the method in the context of inverse scattering for sound waves, and assessed its performance with numerical simulations. Compared to the conventional nonlinear least squares data fit minimization, the new inversion method is almost unaffected by the multiple scattering effects. It recovers robustly the locations, shapes and magnitudes of scatterers in a very small number of iterations.

Acknowledgements. This material is based upon research supported in part by the U.S. Office of Naval Research under award number N00014-17-1-2057 to Borcea and Mamonov. Borcea also acknowledges support from the AFOSR award FA9550-18-1-0131 and Mamonov

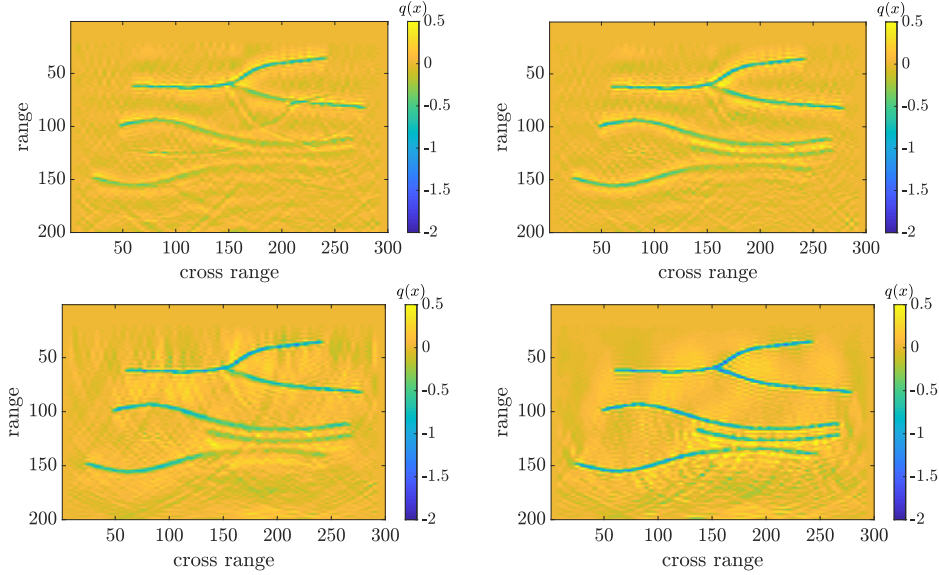


FIG. 4.10. *Inversion results comparison. Top row: LS-RTM with raw data (left plot) and the transformed (Born) data (right plot). Bottom row: ROM-GN after 1 iteration (left plot) and 5 iterations (right plot). The axes are in units of ℓ .*

acknowledges support from the National Science Foundation Grant DMS-1619821.

Appendixes. The next appendixes justify the wave and data model and contain the proofs of the ROM properties stated in Theorems 2.3–2.7 in section 2.4.

Appendix A. The initial condition and data model.

Typically, a wave source is modeled as a force term in the right hand side of the wave equation, and the wave field satisfies homogeneous initial conditions. In this appendix we explain how such a typical formulation can be transformed in problem (1.1)–(1.3) and also justify the data model (1.5).

To simplify the presentation, we assume throughout the appendix that the wave field is scalar (i.e., neglect polarization), so $s = 1, \dots, m$ indexes the location of the point-like sensors in the array which emit the same pulse $f(t)$ supported around $t = 0$. The wave generated by the source at \mathbf{x}_s is denoted by $w^{(s)}(t, \mathbf{x})$ and solves the wave equation

$$\partial_t^2 w^{(s)}(t, \mathbf{x}) + L(q)L(q)^T w^{(s)}(t, \mathbf{x}) = \partial_t f(t) \delta(\mathbf{x} - \mathbf{x}_s), \quad \mathbf{x} \in \Omega, \quad t \in \mathbb{R}, \quad (\text{A.1})$$

$$w^{(s)}(t, \mathbf{x}) = 0, \quad t \ll 0, \quad (\text{A.2})$$

with the same homogeneous boundary conditions as in problem (1.1)–(1.3). We suppose that $f(t)$ is real valued, with non-negative Fourier transform**

$$\hat{f}(\omega) = \int_{-\infty}^{\infty} dt e^{i\omega t} f(t) \geq 0, \quad \forall \omega \in \mathbb{R}. \quad (\text{A.3})$$

**The technical condition (A.3) is needed in the derivation below but it is not a big restriction, because in imaging one usually convolves the received signals with the time reversed version of the emitted waveform. This is known as pulse compression in radar imaging [11], and it is essential because due to antenna power considerations, the emitted waveforms are usually long signals (chirps) $F(t)$. Using the time convolution \star_t they are transformed into short pulses $f(t) = F(-t) \star_t F(t)$ with Fourier transform $\hat{f}(\omega) = |\hat{F}(\omega)|^2 \geq 0$.

We can write formally the explicit expression of $w^{(s)}(t, \mathbf{x})$ using the spectral decomposition of the operator

$$A := L(q)L(q)^T, \quad (\text{A.4})$$

which is self-adjoint and coercive. Following [16, Theorem 4.12] we conclude that the eigenvalues of A are ordered as $0 < \lambda_1 \leq \lambda_2 \leq \dots$, with $\lambda_l \rightarrow \infty$ as $l \rightarrow \infty$, and the eigenfunctions $\{y_l(\mathbf{x})\}_{l \geq 1}$ form a complete orthonormal system in $L^2(\Omega)$. Therefore, we can express the wave as

$$w^{(s)}(t, \mathbf{x}) = f(t) \star_t H(t) \sum_{l=1}^{\infty} \cos(t\sqrt{\lambda_l}) y_l(\mathbf{x}_s) y_l(\mathbf{x}), \quad (\text{A.5})$$

where $H(t)$ is the Heaviside step function.

To derive the initial value problem (1.1)–(1.3), we consider the even extension in time of this wave. Starting from equation (A.5), using the Fourier transform formula

$$\int_{-\infty}^{\infty} dt H(t) \cos(t\sqrt{\lambda_l}) e^{i\omega t} = \frac{\pi}{2} \left[\delta(\omega - \sqrt{\lambda_l}) + \delta(\omega + \sqrt{\lambda_l}) \right] + \frac{i\omega}{\lambda_l - \omega^2},$$

and the assumption that $f(t)$ is real valued, which means in light of (A.3) that $\widehat{f}(\omega) = \widehat{f}(-\omega)$, we obtain the following expression of the even time extension

$$\begin{aligned} w_e^{(s)}(t, \mathbf{x}) &= w^{(s)}(t, \mathbf{x}) + w^{(s)}(-t, \mathbf{x}) = \sum_{l=1}^{\infty} \widehat{f}(\sqrt{\lambda_l}) \cos(t\sqrt{\lambda_l}) y_l(\mathbf{x}_s) y_l(\mathbf{x}) \\ &= \left[\cos(t\sqrt{A}) \widehat{f}(\sqrt{A}) \delta(\cdot - \mathbf{x}_s) \right] (\mathbf{x}), \end{aligned} \quad (\text{A.6})$$

where we use the standard definition of functions of self-adjoint operators.

The data are the matrices $D_j = \left(D_j^{(r,s)} \right)_{1 \leq r,s \leq m}$ with entries defined by this wave evaluated at the receivers,

$$D_j^{(r,s)} = w_e^{(s)}(j\tau, \mathbf{x}_r) = \int_{\Omega} d\mathbf{x} \delta(\mathbf{x} - \mathbf{x}_r) \left[\cos(j\tau\sqrt{A}) \widehat{f}(\sqrt{A}) \delta(\cdot - \mathbf{x}_s) \right] (\mathbf{x}), \quad (\text{A.7})$$

for $j = 0, \dots, 2n - 1$. We can rewrite them in the symmetric form (1.5), in terms of the sensor functions

$$b^{(s)}(\mathbf{x}) = \left[\widehat{f}^{\frac{1}{2}}(\sqrt{A}) \delta(\cdot - \mathbf{x}_s) \right] (\mathbf{x}), \quad (\text{A.8})$$

using the commutation relations

$$\cos(t\sqrt{A}) \widehat{f}(\sqrt{A}) = \widehat{f}^{\frac{1}{2}}(\sqrt{A}) \cos(t\sqrt{A}) \widehat{f}^{\frac{1}{2}}(\sqrt{A}).$$

Note from equation (A.6) that at time $t = 0$,

$$w_e^{(s)}(0, \mathbf{x}) = 2w^{(s)}(0, \mathbf{x}) = \left[\widehat{f}(\sqrt{A}) \delta(\cdot - \mathbf{x}_s) \right] (\mathbf{x}). \quad (\text{A.9})$$

From equation (A.1), the homogeneous initial condition (A.2), the finite speed of propagation and the causality of the wave we know that $w^{(s)}(0, \mathbf{x})$ is supported in the immediate vicinity of \mathbf{x}_s . The sensor function is just like it, but for a different pulse with Fourier transform

$\widehat{f}^{\frac{1}{2}}$. Therefore, it is supported near \mathbf{x}_s , as stated below equation (1.4). Causality also implies that $w_e^{(s)}(0, \mathbf{x})$ and therefore $b^{(s)}(\mathbf{x})$ are not affected by the medium outside the vicinity of \mathbf{x}_s . Therefore, if the medium is known near the sensors, as is usually the case, the functions $b^{(s)}(\mathbf{x})$ can be calculated. This is why we treat them as known throughout the paper.

Appendix B. Proof of Theorem 2.3.

Equation (2.44) follows from the time stepping scheme (2.25–2.27), which is the three term recurrence relation for Chebyshev polynomials

$$\begin{aligned} \mathcal{T}_j(z) &= 2z\mathcal{T}_{j-1}(z) - \mathcal{T}_{j-2}(z), \quad j \geq 1, \\ \mathcal{T}_0(z) &= z^0, \\ \mathcal{T}_{-1}(z) &= \mathcal{T}_1(z), \end{aligned} \quad (\text{B.1})$$

valid for any argument z .

To prove (1.11), we observe that (2.8) implies that the approximation subspace

$$\begin{aligned} \mathfrak{X} &= \text{colspan}\{\mathcal{T}_j(\mathcal{P}(q))\mathbf{b}(\mathbf{x}), j = 0, \dots, n-1\} \\ &= \text{colspan}\{\mathbf{b}(\mathbf{x}), \mathcal{P}(q)\mathbf{b}(\mathbf{x}), \dots, \mathcal{P}(q)^{n-1}\mathbf{b}(\mathbf{x})\} \end{aligned} \quad (\text{B.2})$$

is a block Krylov subspace. Since $\mathfrak{X} = \text{range}(\mathbf{U}(\mathbf{x})) = \text{range}(\mathbf{V}(\mathbf{x}))$, any polynomial $\mathcal{Q}_i(\mathcal{P}(q))\mathbf{b}(\mathbf{x})$ of degree $i \leq n-1$ is represented exactly in \mathfrak{X} , i.e.,

$$\mathcal{Q}_i(\mathcal{P}(q))\mathbf{b}(\mathbf{x}) = \mathbf{V}(\mathbf{x})\mathcal{Q}_i(\mathcal{P}^{\text{ROM}}(q))\mathbf{b}^{\text{ROM}}, \quad 0 \leq i \leq n-1. \quad (\text{B.3})$$

Any Chebyshev polynomial $\mathcal{T}_j(z)$ of degree $j = 0, \dots, 2n-1$ can be represented uniquely (via polynomial division) as

$$\mathcal{T}_j(z) = \mathcal{Q}_i(z)\mathcal{T}_n(z) + \mathcal{R}_k(z), \quad (\text{B.4})$$

for some polynomials $\mathcal{Q}_i(z), \mathcal{R}_k(z)$ of degrees $i, k \leq n-1$. Setting $z = \mathcal{P}(q)$, and using the facts that $\mathcal{Q}_i(\mathcal{P}(q))$ is self-adjoint and $\mathcal{Q}_i(\mathcal{P}^{\text{ROM}}(q))$ is symmetric, we obtain

$$\begin{aligned} D_j &\stackrel{(1.10)}{=} \langle \mathbf{b}, \mathcal{T}_j(\mathcal{P}(q))\mathbf{b} \rangle \\ &\stackrel{(B.4)}{=} \langle \mathbf{b}, \mathcal{Q}_i(\mathcal{P}(q))\mathcal{T}_n(\mathcal{P}(q))\mathbf{b} \rangle + \langle \mathbf{b}, \mathcal{R}_k(\mathcal{P}(q))\mathbf{b} \rangle \\ &\stackrel{(B.1)}{=} \langle \mathcal{Q}_i(\mathcal{P}(q))\mathbf{b}, [2\mathcal{P}(q)\mathcal{T}_{n-1}(\mathcal{P}(q)) - \mathcal{T}_{n-2}(\mathcal{P}(q))]\mathbf{b} \rangle \\ &\quad + \langle \mathbf{b}, \mathcal{R}_k(\mathcal{P}(q))\mathbf{b} \rangle \\ &\stackrel{(B.3)}{=} \langle \mathbf{V}\mathcal{Q}_i(\mathcal{P}^{\text{ROM}}(q))\mathbf{b}^{\text{ROM}}, [2\mathcal{P}(q)\mathbf{V}\mathcal{T}_{n-1}(\mathcal{P}^{\text{ROM}}(q)) - \mathbf{V}\mathcal{T}_{n-2}(\mathcal{P}^{\text{ROM}}(q))]\mathbf{b}^{\text{ROM}} \rangle \\ &\quad + \langle \mathbf{b}, \mathbf{V}\mathcal{R}_k(\mathcal{P}^{\text{ROM}}(q))\mathbf{b}^{\text{ROM}} \rangle \\ &\stackrel{(2.33)}{=} \mathbf{b}^{\text{ROM}T}\mathcal{Q}_i(\mathcal{P}^{\text{ROM}}(q))[2\mathcal{P}^{\text{ROM}}(q)\mathcal{T}_{n-1}(\mathcal{P}^{\text{ROM}}(q)) - \mathcal{T}_{n-2}(\mathcal{P}^{\text{ROM}}(q))]\mathbf{b}^{\text{ROM}} \\ &\quad + \mathbf{b}^{\text{ROM}T}\mathcal{R}_k(\mathcal{P}^{\text{ROM}}(q))\mathbf{b}^{\text{ROM}} \\ &\stackrel{(B.1)}{=} \mathbf{b}^{\text{ROM}T}[\mathcal{Q}_i(\mathcal{P}^{\text{ROM}}(q))\mathcal{T}_n(\mathcal{P}^{\text{ROM}}(q)) + \mathcal{R}_k(\mathcal{P}^{\text{ROM}}(q))]\mathbf{b}^{\text{ROM}} \\ &\stackrel{(B.4)}{=} \mathbf{b}^{\text{ROM}T}\mathcal{T}_j(\mathcal{P}^{\text{ROM}}(q))\mathbf{b}^{\text{ROM}}, \end{aligned}$$

for all $j = 0, \dots, 2n-1$.

Appendix C. Proof of Theorem 2.4.

The symmetry of the ROM propagator follows immediately from equation (2.34), because $\mathcal{P}(q)$ is self-adjoint.

To prove that $\mathcal{P}^{\text{ROM}}(q)$ is block-tridiagonal, it suffices to show

$$\mathcal{P}^{\text{ROM}}(q)_{j+l,j} = \langle \mathbf{v}_{j+l}, \mathcal{P}(q)\mathbf{v}_j \rangle = 0, \quad \forall l = 2, \dots, n-j-1. \quad (\text{C.1})$$

From definition (2.32) of the orthogonal snapshots and the fact that the inverse \mathbf{R}^{-1} of the block upper triangular \mathbf{R} is also block upper triangular, we get

$$\mathbf{v}_j(\mathbf{x}) = \sum_{i=0}^j \mathbf{u}_i(\mathbf{x}) \mathbf{R}_{i,j}^{-1}, \quad j = 0, \dots, n-1.$$

We also have from the time stepping equation (2.5) that

$$\mathcal{P}(q)\mathbf{v}_j(\mathbf{x}) = \sum_{i=0}^j \mathcal{P}(q)\mathbf{u}_i(\mathbf{x}) \mathbf{R}_{i,j}^{-1} = \frac{1}{2} \left[\sum_{i=0}^j \mathbf{u}_{i+1}(\mathbf{x}) \mathbf{R}_{i,j}^{-1} + \sum_{i=0}^j \mathbf{u}_{|i-1|}(\mathbf{x}) \mathbf{R}_{i,j}^{-1} \right],$$

and therefore

$$\begin{aligned} \mathcal{P}^{\text{ROM}}(q)_{j+l,j} &= \langle \mathbf{v}_{j+l}, \mathcal{P}(q)\mathbf{v}_j \rangle = \frac{1}{2} \sum_{i=0}^j \left[\langle \mathbf{v}_{j+l}, \mathbf{u}_{i+1} \rangle + \langle \mathbf{v}_{j+l}, \mathbf{u}_{|i-1|} \rangle \right] \mathbf{R}_{i,j}^{-1} \\ &= \frac{1}{2} \sum_{i=0}^j \left[\mathbf{R}_{j+l,i+1} + \mathbf{R}_{j+l,|i-1|} \right] \mathbf{R}_{i,j}^{-1}, \end{aligned}$$

where the last equality is because $\mathbf{R} = \mathbf{V}^T \mathbf{U}$. Since \mathbf{R} is block upper triangular, the right hand side in this equation is non-zero if the index $j \geq i$ satisfies $j+l \leq i+1$ or $j+l \leq |i-1|$. This is impossible for $l \geq 2$, so result (C.1) holds and $\mathcal{P}^{\text{ROM}}(q)$ is block tridiagonal.

It is clear from the definition (1.9) of the propagator operator $\mathcal{P}(q)$ that its eigenvalues must lie in the interval $[-1, 1]$. Since $\mathcal{P}^{\text{ROM}}(q)$ is the Galerkin projection (2.34) of the propagator, its eigenvalues also lie in $[-1, 1]$. We now prove that

$$\text{Ker}(I - \mathcal{P}(q)) \cap \mathfrak{X} = \{\mathbf{0}\}, \quad (\text{C.2})$$

which implies that

$$\mathbf{I}_{nm} - \mathcal{P}^{\text{ROM}}(q) = \mathbf{V}^T (I - \mathcal{P}(q)) \mathbf{V}$$

is invertible.

Indeed, consider any element in \mathfrak{X} , written as

$$\sum_{j=0}^{n-1} \mathbf{u}_j(\mathbf{x}) \boldsymbol{\alpha}_j \in \mathfrak{X},$$

for $m \times m$ diagonal matrices $\boldsymbol{\alpha}_j$, and suppose that it lies in the kernel of $I - \mathcal{P}(q)$,

$$(I - \mathcal{P}(q)) \sum_{j=0}^{n-1} \mathbf{u}_j(\mathbf{x}) \boldsymbol{\alpha}_j = 0. \quad (\text{C.3})$$

We wish to show that $\boldsymbol{\alpha}_j = \mathbf{0}$, for $j = 0, \dots, n-1$. Using (2.5)–(2.7) in (C.3), we get

$$\sum_{j=0}^{n-1} \left[\mathbf{u}_j(\mathbf{x}) - \frac{\mathbf{u}_{j+1}(\mathbf{x}) + \mathbf{u}_{j-1}(\mathbf{x})}{2} \right] \boldsymbol{\alpha}_j = 0,$$

and reordering the terms and using the initial condition (2.11) we have

$$\begin{aligned} & \mathbf{u}_0(\mathbf{x})\left(\alpha_0 - \frac{\alpha_1}{2}\right) + \mathbf{u}_1(\mathbf{x})\left(\alpha_1 - \alpha_0 - \frac{\alpha_2}{2}\right) + \mathbf{u}_2(\mathbf{x})\left(\alpha_2 - \frac{\alpha_1 + \alpha_3}{2}\right) + \dots \\ & + \mathbf{u}_{n-2}(\mathbf{x})\left(\alpha_{n-2} - \frac{\alpha_{n-3} + \alpha_{n-1}}{2}\right) + \mathbf{u}_{n-1}(\mathbf{x})\left(\alpha_{n-1} - \frac{\alpha_{n-2}}{2}\right) - \mathbf{u}_n(\mathbf{x})\frac{\alpha_{n-1}}{2} = 0. \end{aligned}$$

The wave snapshots are linearly independent up to time $n\tau$ by Assumption 2.1, so we can equate the coefficients in this equation to 0. Starting with $\alpha_{n-1} = \mathbf{0}$ and solving backward, we get that $\alpha_j = \mathbf{0}$, for all $j = 0, \dots, n-1$. This shows that (C.2) holds and completes the proof of the theorem. \square

Appendix D. Proof of Theorem 2.5.

We obtain from definitions (2.12), (2.34) and (2.48) that

$$\frac{2}{\tau^2}(\mathbf{I}_{nm} - \mathcal{P}^{\text{ROM}}(q)) = \mathbf{V}^T \frac{2}{\tau^2}(I - \mathcal{P}(q))\mathbf{V} = \mathbf{V}^T \mathcal{L}(q)\mathcal{L}(q)^T \mathbf{V} = \mathcal{L}^{\text{ROM}}(q)\mathcal{L}^{\text{ROM}}(q)^T, \quad (\text{D.1})$$

where $\mathcal{L}^{\text{ROM}}(q)$ is an $nm \times nm$ block lower bidiagonal, invertible matrix by Theorem 2.4. We use it to define the quasimatrix

$$\widehat{\mathbf{V}}(\mathbf{x}) = \mathcal{L}(q)^T \mathbf{V}(\mathbf{x})\mathcal{L}^{\text{ROM}}(q)^{-T}, \quad (\text{D.2})$$

and write

$$\mathcal{L}^{\text{ROM}}(q) = \mathbf{V}^T \mathcal{L}(q)\widehat{\mathbf{V}}. \quad (\text{D.3})$$

Note that we used in (D.1) the fact that $\mathcal{L}^{\text{ROM}}(q)^T = \widehat{\mathbf{V}}^T \mathcal{L}(q)^T \mathbf{V}$. This can be seen from

$$\begin{aligned} (\mathcal{L}^{\text{ROM}}(q)^T \boldsymbol{\varphi}^{\text{ROM}}, \widehat{\boldsymbol{\varphi}}^{\text{ROM}}) &= (\boldsymbol{\varphi}^{\text{ROM}}, \mathcal{L}^{\text{ROM}}(q)\widehat{\boldsymbol{\varphi}}^{\text{ROM}}) \\ &= (\boldsymbol{\varphi}^{\text{ROM}}, \mathbf{V}^T \mathcal{L}(q)\widehat{\mathbf{V}}\widehat{\boldsymbol{\varphi}}^{\text{ROM}}) \\ &= \langle \mathbf{V}\boldsymbol{\varphi}^{\text{ROM}}, \mathcal{L}(q)\widehat{\mathbf{V}}\widehat{\boldsymbol{\varphi}}^{\text{ROM}} \rangle \\ &= \langle \mathcal{L}(q)^T \mathbf{V}\boldsymbol{\varphi}^{\text{ROM}}, \widehat{\mathbf{V}}\widehat{\boldsymbol{\varphi}}^{\text{ROM}} \rangle \\ &= (\widehat{\mathbf{V}}^T \mathcal{L}(q)^T \mathbf{V}\boldsymbol{\varphi}^{\text{ROM}}, \widehat{\boldsymbol{\varphi}}^{\text{ROM}}), \end{aligned} \quad (\text{D.4})$$

where (\cdot, \cdot) is the inner product in \mathbb{R}^{nm} . Since (D.4) holds for any $\boldsymbol{\varphi}^{\text{ROM}}, \widehat{\boldsymbol{\varphi}}^{\text{ROM}} \in \mathbb{R}^{nm}$, we indeed have

$$\mathcal{L}^{\text{ROM}}(q)^T = \widehat{\mathbf{V}}^T \mathcal{L}(q)^T \mathbf{V}, \quad (\text{D.5})$$

a counterpart of (D.3).

Returning to the quasimatrix $\widehat{\mathbf{V}}(\mathbf{x})$, we observe that it has orthonormal columns

$$\widehat{\mathbf{V}}^T \widehat{\mathbf{V}} = \mathcal{L}^{\text{ROM}}(q)^{-1} \mathbf{V}^T \mathcal{L}(q)\mathcal{L}(q)^T \mathbf{V} \mathcal{L}^{\text{ROM}}(q)^{-T} \stackrel{(\text{D.1})}{=} \mathbf{I}_{nm}, \quad (\text{D.6})$$

and we now show that it satisfies the statement of the theorem.

Recall from (2.37) that the ROM snapshots $\mathbf{u}_j^{\text{ROM}}$, for $j = 0, \dots, n-1$, form the block upper triangular matrix \mathbf{R} . Since $\mathcal{L}^{\text{ROM}}(q)^T$ is block upper bidiagonal, we get from (2.60) that

$$\widehat{\mathbf{u}}_0^{\text{ROM}} = \frac{\tau}{2} \mathcal{L}^{\text{ROM}}(q)^T \mathbf{b}^{\text{ROM}} = \frac{\tau}{2} \mathcal{L}^{\text{ROM}}(q)^T \begin{pmatrix} \mathbf{R}_{0,0} \\ \vdots \\ \mathbf{0} \end{pmatrix} = \begin{pmatrix} \widehat{\mathbf{R}}_{0,0} \\ \vdots \\ \mathbf{0} \end{pmatrix},$$

where the right hand side defines the $m \times m$ matrix $\widehat{\mathbf{R}}_{0,0}$. The next dual snapshot is obtained from equation (2.57),

$$\widehat{\mathbf{u}}_1^{\text{ROM}} = \widehat{\mathbf{u}}_0^{\text{ROM}} + \tau \mathcal{L}^{\text{ROM}}(q)^T \mathbf{u}_1^{\text{ROM}} = \begin{pmatrix} \widehat{\mathbf{R}}_{0,0} \\ \vdots \\ \mathbf{0} \end{pmatrix} + \tau \mathcal{L}^{\text{ROM}}(q)^T \begin{pmatrix} \mathbf{R}_{0,1} \\ \mathbf{R}_{1,1} \\ \mathbf{0} \\ \vdots \\ \mathbf{0} \end{pmatrix} = \begin{pmatrix} \widehat{\mathbf{R}}_{0,1} \\ \widehat{\mathbf{R}}_{1,1} \\ \mathbf{0} \\ \vdots \\ \mathbf{0} \end{pmatrix}$$

and continuing this way we get (2.62), with block upper triangular $\widehat{\mathbf{R}}$.
Next, we show that

$$\widehat{\mathbf{u}}_0 \in \text{range}(\widehat{\mathbf{V}}). \quad (\text{D.7})$$

Indeed, using that $\widehat{\mathbf{V}}\widehat{\mathbf{V}}^T$ is the orthogonal projector on $\text{range}(\widehat{\mathbf{V}})$, we calculate

$$\begin{aligned} \widehat{\mathbf{V}}\widehat{\mathbf{V}}^T \widehat{\mathbf{u}}_0(\mathbf{x}) &\stackrel{(\text{D.2})}{=} \mathcal{L}(q)^T \mathbf{V} \mathcal{L}^{\text{ROM}}(q)^{-T} \mathcal{L}^{\text{ROM}}(q)^{-1} \mathbf{V}^T \mathcal{L}(q) \widehat{\mathbf{u}}_0(\mathbf{x}) \\ &\stackrel{(2.55)}{=} \frac{\tau}{2} \mathcal{L}(q)^T \mathbf{V} \mathcal{L}^{\text{ROM}}(q)^{-T} \mathcal{L}^{\text{ROM}}(q)^{-1} \mathbf{V}^T \mathcal{L}(q) \mathcal{L}(q)^T \mathbf{b}(\mathbf{x}) \\ &= \frac{\tau}{2} \mathcal{L}(q)^T \mathbf{V} \mathcal{L}^{\text{ROM}}(q)^{-T} \mathcal{L}^{\text{ROM}}(q)^{-1} \mathbf{V}^T \mathcal{L}(q) \mathcal{L}(q)^T \mathbf{V} \mathbf{V}^T \mathbf{b}(\mathbf{x}) \end{aligned}$$

where the last equality is because $\mathbf{V}\mathbf{V}^T$ is the orthogonal projector on the space (2.1) to which \mathbf{b} belongs. The right hand side simplifies by equation (D.1), and (D.7) holds because

$$\begin{aligned} \widehat{\mathbf{V}}\widehat{\mathbf{V}}^T \widehat{\mathbf{u}}_0(\mathbf{x}) &= \frac{\tau}{2} \mathcal{L}(q)^T \mathbf{V} \mathcal{L}^{\text{ROM}}(q)^{-T} \mathcal{L}^{\text{ROM}}(q)^{-1} \mathcal{L}^{\text{ROM}}(q) \mathcal{L}^{\text{ROM}}(q)^T \mathbf{V}^T \mathbf{b}(\mathbf{x}) \\ &= \frac{\tau}{2} \mathcal{L}(q)^T \mathbf{V} \mathbf{V}^T \mathbf{b}(\mathbf{x}) = \frac{\tau}{2} \mathcal{L}(q)^T \mathbf{b}(\mathbf{x}) \stackrel{(2.55)}{=} \widehat{\mathbf{u}}_0(\mathbf{x}). \end{aligned}$$

Furthermore, we have

$$\widehat{\mathbf{u}}_0(\mathbf{x}) = \widehat{\mathbf{V}}(\mathbf{x}) \widehat{\mathbf{u}}_0^{\text{ROM}}, \quad (\text{D.8})$$

because

$$\begin{aligned} \widehat{\mathbf{V}}(\mathbf{x}) \widehat{\mathbf{u}}_0^{\text{ROM}} &\stackrel{(2.60)}{=} \frac{\tau}{2} \widehat{\mathbf{V}}(\mathbf{x}) \mathcal{L}^{\text{ROM}}(q)^T \mathbf{b}^{\text{ROM}} \\ &\stackrel{(\text{D.3})}{=} \frac{\tau}{2} \widehat{\mathbf{V}}\widehat{\mathbf{V}}^T \mathcal{L}(q)^T \mathbf{V} \mathbf{b}^{\text{ROM}} \\ &\stackrel{(2.35)}{=} \frac{\tau}{2} \widehat{\mathbf{V}}\widehat{\mathbf{V}}^T \mathcal{L}(q)^T \mathbf{V} \mathbf{V}^T \mathbf{b}(\mathbf{x}) \\ &= \frac{\tau}{2} \widehat{\mathbf{V}}\widehat{\mathbf{V}}^T \mathcal{L}(q)^T \mathbf{b}(\mathbf{x}) \\ &\stackrel{(2.55)}{=} \widehat{\mathbf{V}}\widehat{\mathbf{V}}^T \widehat{\mathbf{u}}_0(\mathbf{x}) \stackrel{(\text{D.7})}{=} \widehat{\mathbf{u}}_0(\mathbf{x}). \end{aligned}$$

Equations (2.37), (2.33) and (2.57) give

$$\mathbf{u}_j(\mathbf{x}) = \mathbf{V} \mathbf{u}_j^{\text{ROM}} = \mathbf{V} \mathcal{L}^{\text{ROM}}(q)^{-T} \left(\frac{\widehat{\mathbf{u}}_j^{\text{ROM}} - \widehat{\mathbf{u}}_{j-1}^{\text{ROM}}}{\tau} \right), \quad j = 0, \dots, n-1,$$

and therefore, by (2.52),

$$\begin{aligned} \frac{\widehat{\mathbf{u}}_j(\mathbf{x}) - \widehat{\mathbf{u}}_{j-1}(\mathbf{x})}{\tau} &= \mathcal{L}(q)^T \mathbf{u}_j(\mathbf{x}) = \mathcal{L}(q)^T \mathbf{V} \mathcal{L}^{\text{ROM}}(q)^{-T} \left(\frac{\widehat{\mathbf{u}}_j^{\text{ROM}} - \widehat{\mathbf{u}}_{j-1}^{\text{ROM}}}{\tau} \right) \\ &\stackrel{(\text{D.3})}{=} \widehat{\mathbf{V}}(\mathbf{x}) \left(\frac{\widehat{\mathbf{u}}_j^{\text{ROM}} - \widehat{\mathbf{u}}_{j-1}^{\text{ROM}}}{\tau} \right), \quad j = 0, \dots, n-1. \end{aligned}$$

Starting with (D.8), this implies that

$$\widehat{\mathbf{u}}_j(\mathbf{x}) = \widehat{\mathbf{V}}(\mathbf{x})\widehat{\mathbf{u}}_j^{\text{ROM}}, \quad j = 0, \dots, n-1. \quad \square$$

Appendix E. Proof of Theorem 2.7.

The block-Lanczos iteration [15, Chapter 4] carried out for the skew adjoint operator

$$\mathfrak{L}(q) = \begin{pmatrix} 0 & -\mathcal{L}(q) \\ \mathcal{L}(q)^T & 0 \end{pmatrix}, \quad (\text{E.1})$$

with a starting vector $[\boldsymbol{\nu}_0^T(\mathbf{x}); \mathbf{0}]^T$ generates the quasimatrix

$$\mathcal{V}(\mathbf{x}) = \begin{pmatrix} \boldsymbol{\nu}_0(\mathbf{x}) & \mathbf{0} & \boldsymbol{\nu}_1(\mathbf{x}) & \mathbf{0} & \dots & \boldsymbol{\nu}_{n-1}(\mathbf{x}) & \mathbf{0} \\ \mathbf{0} & \widehat{\boldsymbol{\nu}}_0(\mathbf{x}) & \mathbf{0} & \widehat{\boldsymbol{\nu}}_1(\mathbf{x}) & \dots & \mathbf{0} & \widehat{\boldsymbol{\nu}}_{n-1}(\mathbf{x}) \end{pmatrix} \quad (\text{E.2})$$

with $2n$ block columns written in terms of some orthonormal snapshots of the form (2.67) and (2.68) that we wish to find. The Lanczos iteration calculates these snapshots so that

$$\mathfrak{L}(q)\mathcal{V}(\mathbf{x}) = \mathcal{V}(\mathbf{x})\widetilde{\mathfrak{L}}(q) + \begin{pmatrix} \mathbf{0} & \dots & \mathbf{0} & \mathbf{r}(\mathbf{x}) \\ \mathbf{0} & \dots & \mathbf{0} & \mathbf{0} \end{pmatrix} \quad (\text{E.3})$$

where $\widetilde{\mathfrak{L}}(q)$ is $2nm \times 2nm$ block tridiagonal, skew-symmetric. Its diagonal consists of zero $m \times m$ blocks and the upper diagonal is, in the MATLAB notation,

$$\text{diag}(\widetilde{\mathfrak{L}}(q), 1) = (-\boldsymbol{\Lambda}_{0,0}^{\text{ROM}}(q), \boldsymbol{\Lambda}_{1,0}^{\text{ROM}}(q)^T, -\boldsymbol{\Lambda}_{1,1}^{\text{ROM}}(q), \boldsymbol{\Lambda}_{2,1}^{\text{ROM}}(q)^T, \dots, -\boldsymbol{\Lambda}_{n-1,n-1}^{\text{ROM}}(q)), \quad (\text{E.4})$$

where $\boldsymbol{\Lambda}_{i,j}^{\text{ROM}}(q)$ are the $m \times m$ blocks of (2.69). The last term in (E.3) is the residual quasimatrix, with the single $m \times m$ non-zero block $\mathbf{r}(\mathbf{x})$. In this proof we will relate the $\boldsymbol{\nu}_j$ and $\widehat{\boldsymbol{\nu}}_j$ to the fields $\boldsymbol{\varphi}_j$ and $\widehat{\boldsymbol{\varphi}}_j$ from (2.70) and (2.71). Further, the entries of the matrix $\widetilde{\mathfrak{L}}$ will be related to the block-finite difference coefficients $\boldsymbol{\Gamma}_j$ and $\widehat{\boldsymbol{\Gamma}}_j$.

Equating the left and right hand sides of the Lanczos decomposition in (E.3) block column-wise, we obtain the following recursion scheme

$$\mathcal{L}(q)\widehat{\boldsymbol{\nu}}_j(\mathbf{x}) = \boldsymbol{\nu}_j(\mathbf{x})\boldsymbol{\Lambda}_{j,j}^{\text{ROM}}(q) + \boldsymbol{\nu}_{j+1}(\mathbf{x})\boldsymbol{\Lambda}_{j+1,j}^{\text{ROM}}(q), \quad (\text{E.5})$$

$$\mathcal{L}(q)^T \boldsymbol{\nu}_j(\mathbf{x}) = \widehat{\boldsymbol{\nu}}_{j-1}(\mathbf{x})\boldsymbol{\Lambda}_{j,j-1}^{\text{ROM}}(q)^T + \widehat{\boldsymbol{\nu}}_j(\mathbf{x})\boldsymbol{\Lambda}_{j,j}^{\text{ROM}}(q)^T, \quad (\text{E.6})$$

for $j = 0, \dots, n-1$, where

$$\widehat{\boldsymbol{\nu}}_{-1}(\mathbf{x}) = \mathbf{0}, \quad \boldsymbol{\nu}_n(\mathbf{x})\boldsymbol{\Lambda}_{n,n-1}^{\text{ROM}}(q) = -\mathbf{r}(\mathbf{x}).$$

The matrices $\boldsymbol{\Lambda}^{\text{ROM}}$ follow from the normalization and orthogonality conditions for $\boldsymbol{\nu}_j$ and $\widehat{\boldsymbol{\nu}}_j$. We note that the recursion relations in (E.5) and (E.6) resemble the recursion relations of a finite difference time-stepping scheme. We wish to write $\boldsymbol{\nu}_j(\mathbf{x})$ and $\widehat{\boldsymbol{\nu}}_j(\mathbf{x})$ in the form

$$\boldsymbol{\nu}_j(\mathbf{x}) = \boldsymbol{\varphi}_j(\mathbf{x})\sqrt{\boldsymbol{\gamma}_j}, \quad \widehat{\boldsymbol{\nu}}_j(\mathbf{x}) = \widehat{\boldsymbol{\varphi}}_j(\mathbf{x})\sqrt{\boldsymbol{\gamma}_j}, \quad (\text{E.7})$$

for some arbitrary choice of the square roots

$$\boldsymbol{\gamma}_j = \sqrt{\boldsymbol{\gamma}_j}\sqrt{\boldsymbol{\gamma}_j}^T, \quad \widehat{\boldsymbol{\gamma}}_j = \sqrt{\widehat{\boldsymbol{\gamma}}_j}\sqrt{\widehat{\boldsymbol{\gamma}}_j}^T, \quad j \geq 0. \quad (\text{E.8})$$

For any such choice we have,

$$\begin{aligned}\langle \boldsymbol{\nu}_j, \boldsymbol{\nu}_j \rangle &\stackrel{\text{(E.7)}}{=} \sqrt{\widehat{\gamma}_j}^T \langle \boldsymbol{\varphi}_j, \boldsymbol{\varphi}_j \rangle \sqrt{\widehat{\gamma}_j} \stackrel{\text{(2.73)}}{=} \sqrt{\widehat{\gamma}_j}^T \widehat{\gamma}_j^{-1} \sqrt{\widehat{\gamma}_j} \stackrel{\text{(E.8)}}{=} \mathbf{I}_m \\ \langle \widehat{\boldsymbol{\nu}}_j, \widehat{\boldsymbol{\nu}}_j \rangle &= \sqrt{\boldsymbol{\gamma}_j}^T \langle \widehat{\boldsymbol{\varphi}}_j, \widehat{\boldsymbol{\varphi}}_j \rangle \sqrt{\boldsymbol{\gamma}_j} = \sqrt{\boldsymbol{\gamma}_j}^T \boldsymbol{\gamma}_j^{-1} \sqrt{\boldsymbol{\gamma}_j} = \mathbf{I}_m,\end{aligned}$$

for $j = 0, \dots, n-1$, so the columns of $\boldsymbol{\nu}_j(\mathbf{x})$ and of $\widehat{\boldsymbol{\nu}}_j(\mathbf{x})$ are orthogonal, as needed.

Substituting (2.75) in (2.70–2.71), we get the equations

$$\left[\boldsymbol{\nu}_{j+1}(\mathbf{x}) \sqrt{\widehat{\gamma}_{j+1}}^{-1} - \boldsymbol{\nu}_j(\mathbf{x}) \sqrt{\widehat{\gamma}_j}^{-1} \right] \boldsymbol{\gamma}_j^{-1} = -\mathcal{L}(q) \widehat{\boldsymbol{\nu}}_j(\mathbf{x}) \sqrt{\boldsymbol{\gamma}_j}^{-1}, \quad (\text{E.9})$$

$$\left[\widehat{\boldsymbol{\nu}}_j(\mathbf{x}) \sqrt{\boldsymbol{\gamma}_j}^{-1} - \widehat{\boldsymbol{\nu}}_{j-1}(\mathbf{x}) \sqrt{\boldsymbol{\gamma}_{j-1}}^{-1} \right] \widehat{\boldsymbol{\gamma}}_j^{-1} = \mathcal{L}(q)^T \boldsymbol{\nu}_j(\mathbf{x}) \sqrt{\widehat{\gamma}_j}^{-1}, \quad (\text{E.10})$$

which must be consistent with (2.70–2.71) and the orthogonality of $\{\boldsymbol{\nu}_j(\mathbf{x})\}_{0 \leq j \leq n-1}$ and of $\{\widehat{\boldsymbol{\nu}}_j(\mathbf{x})\}_{0 \leq j \leq n-1}$. Equations (E.5) and (E.9) are consistent if the blocks of $\boldsymbol{\Lambda}^{\text{ROM}}(q)$ satisfy

$$\boldsymbol{\Lambda}_{j,j}^{\text{ROM}}(q) \stackrel{\text{(E.5)}}{=} \langle \boldsymbol{\nu}_j, \mathcal{L}(q) \widehat{\boldsymbol{\nu}}_j \rangle \stackrel{\text{(E.9)}}{=} \langle \boldsymbol{\nu}_j, \boldsymbol{\nu}_j \rangle \sqrt{\widehat{\gamma}_j}^{-1} \boldsymbol{\gamma}_j^{-1} \sqrt{\boldsymbol{\gamma}_j} = \sqrt{\widehat{\gamma}_j}^{-1} \sqrt{\boldsymbol{\gamma}_j}^{-T}, \quad (\text{E.11})$$

and

$$\begin{aligned}\boldsymbol{\Lambda}_{j+1,j}^{\text{ROM}}(q) &\stackrel{\text{(E.5)}}{=} \langle \boldsymbol{\nu}_{j+1}, \mathcal{L}(q) \widehat{\boldsymbol{\nu}}_j \rangle \stackrel{\text{(E.9)}}{=} -\langle \boldsymbol{\nu}_{j+1}, \boldsymbol{\nu}_{j+1} \rangle \sqrt{\widehat{\gamma}_{j+1}}^{-1} \boldsymbol{\gamma}_j^{-1} \sqrt{\boldsymbol{\gamma}_j} \\ &= -\sqrt{\widehat{\gamma}_{j+1}}^{-1} \sqrt{\boldsymbol{\gamma}_j}^{-T}.\end{aligned} \quad (\text{E.12})$$

The consistency of equations (E.6) and (E.10), which involve the transposed blocks of $\boldsymbol{\Lambda}^{\text{ROM}}(q)$, follows the same way.

Next, we relate \boldsymbol{v}_j to $\boldsymbol{\nu}_j$ by showing that the orthonormal vectors (E.7) satisfy the relations (2.67) and (2.68). To this effect, we note from definitions (2.21), (2.24), (2.31), (2.73) and (2.75) that

$$\boldsymbol{v}_0(\mathbf{x}) = \mathbf{u}_0(\mathbf{x}) \mathbf{R}_{0,0}^{-1} = \mathbf{b}(\mathbf{x}) \mathbf{R}_{0,0}^{-1}, \quad \boldsymbol{\nu}_0(\mathbf{x}) \stackrel{\text{(E.7)}}{=} \boldsymbol{\varphi}_0(\mathbf{x}) \sqrt{\widehat{\gamma}_0} \stackrel{\text{(2.72)}}{=} \mathbf{b}(\mathbf{x}) \sqrt{\widehat{\gamma}_0}. \quad (\text{E.13})$$

Therefore, the columns of $\boldsymbol{\nu}_0(\mathbf{x})$ and $\boldsymbol{v}_0(\mathbf{x})$ are an orthonormal basis of the same space $\text{span}\{\mathbf{u}_0(\mathbf{x})\}$, so the two must be related by an orthogonal transformation $\mathbf{Y}_0 \in \mathbb{R}^{m \times m}$,

$$\boldsymbol{\nu}_0(\mathbf{x}) = \boldsymbol{v}_0(\mathbf{x}) \mathbf{Y}_0. \quad (\text{E.14})$$

We also get from equations (2.61), (2.55) and (2.71) evaluated at $j = 0$ that

$$\widehat{\boldsymbol{v}}_0(\mathbf{x}) = \widehat{\mathbf{u}}_0 \widehat{\mathbf{R}}_{0,0}^{-1}, \quad \widehat{\boldsymbol{\varphi}}_0(\mathbf{x}) = \mathcal{L}(q)^T \mathbf{b}(\mathbf{x}) \widehat{\boldsymbol{\gamma}}_0 = \frac{2}{\tau} \widehat{\mathbf{u}}_0(\mathbf{x}) \widehat{\boldsymbol{\gamma}}_0,$$

so the columns of $\widehat{\boldsymbol{\nu}}_0(\mathbf{x})$ and $\widehat{\boldsymbol{v}}_0(\mathbf{x})$ are orthonormal bases of the same space $\text{span}\{\widehat{\mathbf{u}}_0(\mathbf{x})\}$, and must be related by an orthogonal transformation $\widehat{\mathbf{Y}}_0 \in \mathbb{R}^{m \times m}$,

$$\widehat{\boldsymbol{\nu}}_0(\mathbf{x}) = \widehat{\boldsymbol{v}}_0(\mathbf{x}) \widehat{\mathbf{Y}}_0. \quad (\text{E.15})$$

Then, equations (2.36) and (2.51) and (2.70) for $j = 0$ give that

$$\boldsymbol{v}_1(\mathbf{x}) \in \text{span}\{\mathbf{u}_0(\mathbf{x}), \mathbf{u}_1(\mathbf{x})\}, \quad \boldsymbol{\nu}_1(\mathbf{x}) \in \text{span}\{\mathbf{u}_0(\mathbf{x}), \mathbf{u}_1(\mathbf{x})\},$$

so the columns of $\boldsymbol{\nu}_1(\mathbf{x})$ and $\mathbf{v}_1(\mathbf{x})$ are orthonormal bases of the same space, the orthogonal complement of $\text{span}\{\mathbf{u}_0(\mathbf{x})\}$ in $\text{span}\{\mathbf{u}_0(\mathbf{x}), \mathbf{u}_1(\mathbf{x})\}$. Therefore, they must be related by an orthogonal transformation $\mathbf{Y}_1 \in \mathbb{R}^{m \times m}$,

$$\boldsymbol{\nu}_1(\mathbf{x}) = \mathbf{v}_1(\mathbf{x})\mathbf{Y}_1. \quad (\text{E.16})$$

Iterating this way we obtain the relations (2.67) and (2.68).

Using these orthogonal block diagonal transformations $\mathbf{Y} = \text{diag}(\mathbf{Y}_0, \dots, \mathbf{Y}_{n-1})$ and $\widehat{\mathbf{Y}} = \text{diag}(\widehat{\mathbf{Y}}_0, \dots, \widehat{\mathbf{Y}}_{n-1})$, we can now define the matrices

$$\boldsymbol{\Gamma}_j = \sqrt{\gamma_j} \widehat{\mathbf{Y}}_j^T, \quad \widehat{\boldsymbol{\Gamma}}_j = \sqrt{\widehat{\gamma}_j} \mathbf{Y}_j^T, \quad j \geq 0, \quad (\text{E.17})$$

which are also square roots of γ_j and $\widehat{\gamma}_j$,

$$\begin{aligned} \boldsymbol{\Gamma}_j \boldsymbol{\Gamma}_j^T &= \sqrt{\gamma_j} \widehat{\mathbf{Y}}_j^T \widehat{\mathbf{Y}}_j \sqrt{\gamma_j} = \sqrt{\gamma_j} \sqrt{\gamma_j} \stackrel{(\text{E.8})}{=} \gamma_j, \\ \widehat{\boldsymbol{\Gamma}}_j \widehat{\boldsymbol{\Gamma}}_j^T &= \sqrt{\widehat{\gamma}_j} \mathbf{Y}_j^T \mathbf{Y}_j \sqrt{\widehat{\gamma}_j} = \sqrt{\widehat{\gamma}_j} \sqrt{\widehat{\gamma}_j} \stackrel{(\text{E.8})}{=} \widehat{\gamma}_j, \quad j \geq 0. \end{aligned}$$

With these matrices the orthogonalized primary and dual snapshots \mathbf{v}_j and $\widehat{\mathbf{v}}_j$ can be shown to be transforms of $\boldsymbol{\varphi}_j$ and $\widehat{\boldsymbol{\varphi}}_j$ from (2.70–2.71). We have

$$\begin{aligned} \mathbf{v}_j(\mathbf{x}) &\stackrel{(2.67)}{=} \boldsymbol{\nu}_j(\mathbf{x}) \mathbf{Y}_j^T \stackrel{(\text{E.7})}{=} \boldsymbol{\varphi}_j(\mathbf{x}) \sqrt{\widehat{\gamma}_j} \mathbf{Y}_j^T = \boldsymbol{\varphi}_j(\mathbf{x}) \widehat{\boldsymbol{\Gamma}}_j, \\ \widehat{\mathbf{v}}_j(\mathbf{x}) &\stackrel{(2.68)}{=} \widehat{\boldsymbol{\nu}}_j(\mathbf{x}) \widehat{\mathbf{Y}}_j^T \stackrel{(\text{E.7})}{=} \widehat{\boldsymbol{\varphi}}_j(\mathbf{x}) \sqrt{\gamma_j} \widehat{\mathbf{Y}}_j^T = \widehat{\boldsymbol{\varphi}}_j(\mathbf{x}) \boldsymbol{\Gamma}_j, \end{aligned}$$

and the block lower bidiagonal ROM matrix $\mathcal{L}^{\text{ROM}}(q)$ follows from (2.69) and (E.11–E.12),

$$\begin{aligned} \mathcal{L}^{\text{ROM}}(q)_{j,j} &= \mathbf{Y}_j \boldsymbol{\Lambda}_{j,j}^{\text{ROM}}(q) \widehat{\mathbf{Y}}_j^T \stackrel{(\text{E.11})}{=} \mathbf{Y}_j \sqrt{\widehat{\gamma}_j}^{-1} \sqrt{\gamma_j}^{-T} \widehat{\mathbf{Y}}_j^T \stackrel{(\text{E.17})}{=} \widehat{\boldsymbol{\Gamma}}_j^{-1} \boldsymbol{\Gamma}_j^{-T}, \\ \mathcal{L}^{\text{ROM}}(q)_{j+1,j} &= \mathbf{Y}_{j+1} \boldsymbol{\Lambda}_{j+1,j}^{\text{ROM}}(q) \widehat{\mathbf{Y}}_j^T \stackrel{(\text{E.11})}{=} -\mathbf{Y}_{j+1} \sqrt{\widehat{\gamma}_{j+1}}^{-1} \sqrt{\gamma_j}^{-T} \widehat{\mathbf{Y}}_j^T \stackrel{(\text{E.17})}{=} -\widehat{\boldsymbol{\Gamma}}_{j+1}^{-1} \boldsymbol{\Gamma}_j^{-T}, \end{aligned}$$

which allows an interpretation of the block entries of the ROM as block finite-difference coefficients. This completes the proof of the theorem. \square

REFERENCES

- [1] G. BEYLKIN, *Imaging of discontinuities in the inverse scattering problem by inversion of a causal generalized radon transform*, Journal of Mathematical Physics, 26 (1985), pp. 99–108.
- [2] G. BEYLKIN AND R. BURRIDGE, *Linearized inverse scattering problems in acoustics and elasticity*, Wave motion, 12 (1990), pp. 15–52.
- [3] B. BIONDI, *3D seismic imaging*, vol. 14, Society of Exploration Geophysicists Tulsa, 2006.
- [4] N. BLEISTEIN, J. COHEN, AND W. JOHN JR, *Mathematics of multidimensional seismic imaging, migration, and inversion*, vol. 13, Springer Science & Business Media, 2013.
- [5] L. BORCEA, V. DRUSKIN, A. MAMONOV, AND M. ZASLAVSKY, *Untangling the nonlinearity in inverse scattering with data-driven reduced order models*, Inverse Problems, (2018).
- [6] ———, *Robust nonlinear processing of active array data in inverse scattering via truncated reduced order models*, Journal of Computational Physics, 381 (2019), pp. 1–26.
- [7] M. BORN AND E. WOLF, *Principles of optics: electromagnetic theory of propagation, interference and diffraction of light*, Cambridge University Press, Cambridge, UK, 7 ed., 2002.
- [8] M. CHENEY AND B. BORDEN, *Fundamentals of radar imaging*, vol. 79, Siam, 2009.
- [9] J. CLAERBOUT, *Imaging the earth's interior*, vol. 1, Blackwell scientific publications Oxford, 1985.
- [10] M. COLLINS AND W. KUPERMAN, *Inverse problems in ocean acoustics*, Inverse Problems, 10 (1994), p. 1023.

- [11] J. CURLANDER AND R. McDONOUGH, *Synthetic aperture radar*, vol. 396, John Wiley & Sons New York, NY, USA, 1991.
- [12] W. DAI, P. FOWLER, AND G. T. SCHUSTER, *Multi-source least-squares reverse time migration*, *Geophysical Prospecting*, 60 (2012), pp. 681–695.
- [13] V. DRUSKIN, A. MAMONOV, A. THALER, AND M. ZASLAVSKY, *Direct, nonlinear inversion algorithm for hyperbolic problems via projection-based model reduction*, *SIAM Journal on Imaging Sciences*, 9 (2016), pp. 684–747.
- [14] V. DRUSKIN, A. MAMONOV, AND M. ZASLAVSKY, *A nonlinear method for imaging with acoustic waves via reduced order model backprojection*, *SIAM Journal on Imaging Sciences*, 11 (2018), pp. 164–196.
- [15] G. GOLUB AND C. VAN LOAN, *Matrix Computations*, The Johns Hopkins University Press, Baltimore, MD, 3 ed., 1996.
- [16] W. MCLEAN, *Strongly elliptic systems and boundary integral equations*, Cambridge university press, 2000.
- [17] T. NEMETH, C. WU, AND G. T. SCHUSTER, *Least-squares migration of incomplete reflection data*, *Geophysics*, 64 (1999), pp. 208–221.
- [18] J. NOCEDAL AND S. WRIGHT, *Numerical optimization*, Springer Science & Business Media, New York, NY, 2 ed., 2006.
- [19] T. RIVLIN, *Chebyshev polynomials: From Approximation Theory to Algebra and Number Theory*, Pure Appl. Math. Wiley, New York, 2 ed., 1990.
- [20] L. SCHMERR, *Fundamentals of ultrasonic nondestructive evaluation*, Springer, 2016.
- [21] G. W. STEWART, *Afternotes goes to graduate school: lectures on advanced numerical analysis*, vol. 58, SIAM, 1998.
- [22] W. SYMES, *Migration velocity analysis and waveform inversion*, *Geophysical prospecting*, 56 (2008), pp. 765–790.
- [23] ———, *The seismic reflection inverse problem*, *Inverse problems*, 25 (2009), p. 123008 (39 pp.).
- [24] T. SZABO, *Diagnostic ultrasound imaging: inside out*, Academic Press, 2004.
- [25] A. TARANTOLA, *Inversion of seismic reflection data in the acoustic approximation*, *Geophysics*, 49 (1984), pp. 1259–1266.
- [26] J. VIRIEUX AND S. OPERTO, *An overview of full-waveform inversion in exploration geophysics*, *Geophysics*, 74 (2009), pp. WCC1–WCC26.